

Dark Matter Searches with Astroparticle Data

T. A. PORTER,¹ R. P. JOHNSON,² AND P. W. GRAHAM³

[1] Hansen Experimental Physics Laboratory, Stanford University, Stanford, California 94305; email: tporter@stanford.edu

[2] Santa Cruz Institute for Particle Physics, University of California, Santa Cruz, California 95064; email: rjohnson@scipp.ucsc.edu

[3] Stanford Institute for Theoretical Physics, Stanford University, Stanford, California 94305; email: pwgraham@stanford.edu

Key Words astroparticle physics, elementary particles, galaxies: interstellar medium, gamma rays: diffuse background, gamma rays: galaxies, gamma rays: galaxies: clusters, gamma rays: observations, ISM: cosmic rays, theory

Abstract The existence of dark matter (DM) was first noticed by Zwicky in the 1930s, but its nature remains one of the great unsolved problems of physics. A variety of observations indicate that it is non-baryonic and non-relativistic. One of the preferred candidates for non-baryonic DM is a weakly interacting massive particle (WIMP) that in most models is stable. WIMP self-annihilation can produce cosmic rays, gamma rays, and other particles with signatures that may be detectable. Hints of anomalous cosmic-ray spectra found by recent experiments, such as PAMELA, have motivated interesting interpretations in terms of DM annihilation and/or decay. However, these signatures also have standard astrophysical interpretations, so additional evidence is needed in order to make a case for detection of DM annihilation or decay. Searches by the *Fermi*-LAT for gamma-ray signals from clumps, nearby dwarf spheroidal galaxies, and galaxy clusters have also been performed, along with measurements of the diffuse Galactic and extragalactic gamma-ray emission. In addition, Imaging Air Cherenkov Telescopes like HESS, MAGIC, and VERITAS have reported on searches for gamma-ray emission from dwarf galaxies. In this review, we examine the status of searches for particle DM by these instruments and discuss the interpretations and resulting DM limits.

CONTENTS

INTRODUCTION	2
General Properties of Dark Matter	3
Dark Matter Signals	4
Detectability	5
Other Indirect Dark Matter Signals	8

EXPERIMENTS	9
<i>Cosmic-Ray Instruments: 1960s to Early 2000s</i>	10
<i>Current Cosmic-Ray and Gamma-Ray Experiments</i>	11
<i>Neutrinos</i>	14
RECENT DATA AND INTERPRETATIONS	14
<i>Cosmic Rays</i>	14
<i>Galactic Diffuse Emission</i>	21
<i>Extragalactic Diffuse Emission</i>	26
<i>Gamma-Ray Line Searches</i>	29
<i>Gamma Rays from Dwarf Spheroidal Galaxies and Satellites</i>	30
<i>Galaxy Clusters</i>	37
OUTLOOK	40

1 INTRODUCTION

The combination of many observations, including galactic rotation curves, gravitational lensing, the cosmic microwave background (CMB), and primordial light element abundances, cannot be explained without extending the standard model of particle physics. The simplest extensions involve dark matter (DM) composed of a new particle that may annihilate or decay to standard model particles detectable far from their source. Although there are many other motivations for physics beyond the standard model, astrophysics observations provide some of the few pieces of direct evidence that there must be new physics, thus making the search for signatures of particle DM an especially compelling area of research.

In this review, we examine recent astroparticle experiments and data that seek to discover the particle nature of DM and determine its properties indirectly through the detection of cosmic ray (CR), gamma ray, and neutrino signatures. Such work is complementary to direct and accelerator-based searches, because it is unlikely that enough information will be obtained from a single method alone to determine all of the DM properties. For example, accelerators may detect new candidate particles but cannot ascertain whether they form the DM. Direct and indirect detection experiments rely on different unknown properties of particle DM, so it is important to pursue both. See, e.g., Baltz et al. (2006) and Hooper & Baltz (2008) for comprehensive discussions of how the DM particle sector might eventually be understood by following these complementary avenues of research. DM searches with astroparticle data have the potential to determine the astrophysical distribution of the DM particles, which is not possible with the other methods.

We give a general overview of DM characteristics and popular models, and discuss the recent astroparticle experimental searches for evidence of its particle nature. However, the subject has a large literature and we cannot possibly cover it in entirety here. We refer readers to the extensive reviews by Jungman et al. (1996), Bergström (2000), Bertone, Hooper & Silk (2005), and Feng (2010) (and references therein) for additional background information.

1.1 General Properties of Dark Matter

The approximate distribution of DM in our Universe can be deduced from its gravitational effects, but its nature and microphysical properties are still unknown. There are constraints on the properties of DM particle candidates that strongly favor or rule out various models. Non-gravitational interactions between DM and standard model particles are highly constrained by the lack of observations of particle DM. This strongly disfavors DM that is electrically charged or interacts by the strong nuclear force. In addition, DM must clump gravitationally to form galaxies. This requires DM to be “cold”, that is, nonrelativistic at the time of structure formation, or possibly “warm”. But “hot” DM, that is, relativistic during structure formation, cannot explain the ensemble of data (although some hot DM certainly exists in the form of neutrinos). Within these constraints, the theoretically best-motivated candidates for a DM particle are a weakly interacting massive particle (WIMP) or an axion. (See Feng (2010) for a recent review of some other candidate particles.)

The axion was originally postulated as a solution to the strong CP problem (Peccei & Quinn, 1977; Wilczek, 1978; Weinberg, 1978). The review by Asztalos et al. (2006) discusses axion DM, and we refer readers to that. We do not discuss axions in this review, except to note that one of the few current experiments that can detect axion DM is the Axion Dark Matter eXperiment (ADMX). Unfortunately this instrument will explore only a fraction of the possible axion parameter space (Asztalos et al., 2010).

Typically WIMPs are considered to be thermal relics left over from the early Universe. The interactions of WIMPs with standard model particles kept them in thermal equilibrium at the high temperatures that existed at that time. As the Universe expanded the rate of these interactions, formation and annihilation, eventually became too low, and the WIMP abundance froze out. Thereafter their total number in the Universe no longer changed significantly. (Even a decaying WIMP would have a lifetime bounded to be much longer than the age of the universe, so only a negligible fraction would have decayed by now.) Therefore, the abundance today is inversely proportional to the WIMP self-annihilation cross section. The fractional abundance, relative to the critical density $3H^2/8\pi G$, is

$$\Omega_{\text{WIMP}} \approx \frac{0.1}{h^2} \left(\frac{3 \times 10^{-26} \text{ cm}^3 \text{ s}^{-1}}{\langle \sigma v \rangle} \right) \quad (1)$$

where $\langle \sigma v \rangle$ is the DM annihilation cross section times the relative velocity of two WIMPs averaged over their velocity distribution, and $0.1/h^2$ is the approximate observed abundance of DM (Komatsu et al., 2010). Note that this depends on the DM annihilation cross section and fundamental constants but not on a DM particle mass.

Therefore, to reproduce the observed DM density of our Universe, a WIMP of any mass must have an annihilation cross section of

$$\langle \sigma v \rangle \approx 3 \times 10^{-26} \text{ cm}^3 \text{ s}^{-1}. \quad (2)$$

(There is some small model-dependency in the precise cross section that yields

the observed DM abundance, but it is always quite close to this value.) Because this is a typical value expected for a particle with mass near the weak scale [$\mathcal{O}(100\text{ GeV})$], or with interactions suppressed by that scale, there is a strong motivation to consider DM models in which the candidate particle interacts with a weak force and has a mass around the weak scale. The fact that the observed abundance of DM points to new physics at the weak scale, completely independent of particle physics motivations for new physics at the same scale, is the so-called WIMP miracle (see the review by Feng, 2010, and the discussion therein).

Thus, the WIMP provides a well-motivated DM candidate. Its couplings to the standard model particles are weak, often literally through the weak nuclear force. It most likely has a mass near the weak scale, though much lighter or heavier particles are possible. In fact, the only real bound on a thermal relic DM particle is that it should be heavier than $\sim \text{keV}$ so that it is cold instead of hot DM. Also, its mass should be $\lesssim 300 \text{ TeV}$ to avoid generating more than the observed DM abundance (Griest & Kamionkowski, 1990), though both these limits are somewhat model-dependent. However, the best motivated mass range for the WIMP is within an order of magnitude around $\sim 100 \text{ GeV}$, so we focus on that range in this review.

1.2 Dark Matter Signals

In order for the WIMP miracle to explain the DM abundance, the WIMP must self-annihilate into standard model particles with a cross section close to that given by Equation 2. Importantly, in most particle physics models the annihilation cross section is dominantly s-wave, that is, the leading order behavior of the cross section is $\sigma \sim 1/v$ and hence Equation 2 is independent of the velocity. Therefore, the current value of Equation 2 is the same as in the early Universe (when the DM abundance was set), allowing us to predict the (approximate) annihilation rate at the present epoch. Although the annihilation rate is small now, and no longer affects the overall WIMP abundance, it may be large enough to be observed. The detectable stable end products include photons, neutrinos, electrons, protons, deuterium, and their corresponding antiparticles. Because the annihilations produce equal amounts of matter and antimatter, antimatter is a much better signal due to its significantly lower astrophysical backgrounds.

There is no unique DM signal prediction, because the types and quantities of CRs and other particles produced in the annihilation depend sensitively on the nature of a DM particle candidate and the strengths of its interactions with standard model particles. However, for a particular DM model, it is possible to make predictions that are potentially testable. Two of the more popular DM frameworks that have been tested are the minimal supersymmetric standard model (MSSM) and universal extra dimensions.

The MSSM (Dimopoulos & Georgi, 1981) provides a solution to the standard model hierarchy problem—the smallness of the weak scale relative to the Planck scale—by adding a new fundamental symmetry to the standard model: supersymmetry. This introduces a new partner with mass around the weak scale for every known particle in the standard model. Of these, the lightest supersymmet-

ric partner is stable, making it a good DM candidate. The nature of the lightest supersymmetric partner is determined by its standard model partner, usually the Higgs or neutral gauge boson (corresponding to the higgsino or gaugino, respectively, or mixtures of those known as “neutralinos”). The annihilation products depend on the lightest supersymmetric partner, its mass, and the mass spectrum of the other new particles in the MSSM, leading to significant model dependence even within the MSSM framework.

Universal extra dimensions (Appelquist, Cheng & Dobrescu, 2001) are a commonly discussed extra-dimensional scenario. For this framework, there is a tower of Kaluza-Klein partners for every standard model particle. These are the extra-dimensional momentum modes of the standard model particles and have masses that are multiples of the inverse size of the compact extra dimensions, usually taken to be around the weak scale. In most versions of this theory, the lightest Kaluza-Klein particle is stable, making it a good DM candidate. Its annihilation products can then be predicted for any particular model.

There is also the possibility that DM particle candidates, although cosmologically long-lived, may nevertheless decay, analogous to proton decay in grand unified theories (Arvanitaki et al., 2009). Assuming a similar mechanism for WIMP decay, theory suggests a lifetime of around 10^{27} s. Interestingly, for WIMP masses $\mathcal{O}(1 \text{ TeV})$, the rate of decay products per unit volume in that case would be similar to that from DM annihilation, and therefore may also be observable.

1.3 Detectability

The detectability of a DM signal from annihilation or decay depends on the types of standard model particles, their energies, and where they are produced. Particle physics describes the source spectrum for standard model particle species $s = \gamma, e^\pm, \dots$ in terms of a sum over all possible annihilation final states f , each with branching fraction $B_{f,s}$:

$$\Phi_s(E) = \frac{1}{4\pi} \frac{\langle \sigma v \rangle}{2M_\chi^2} \sum_f \frac{dN_f}{dE} B_{f,s}, \quad (3)$$

where E is the secondary particle energy, M_χ is the WIMP mass, and dN_f/dE is the production rate per annihilation of species f . Substituting $\langle \sigma v \rangle / 2M_\chi^2 \rightarrow \Gamma / M_\chi$, where Γ is the decay rate, gives the corresponding production spectrum for decaying DM.

DM may annihilate or decay to any of the standard model particles: quarks (u, d, c, s, t, b), leptons ($e, \mu, \tau, \nu_e, \nu_\mu, \nu_\tau$), or gauge bosons (W, Z , gluon, photon). For annihilations the final state is often a particle and its antiparticle, though for either annihilations or decays the final state can be more complicated, e.g., three-body. Most of these particles decay rapidly, leaving only the few stable particles and their antiparticles: photons, protons and antiprotons (p/\bar{p}), electrons and positrons (e^\pm), and the three flavors of neutrino (ν_e, ν_μ, ν_τ). Note that it may also be possible to produce a deuterium or anti-deuterium nucleus (D/\bar{D}), which may be detectable with the Advanced Magnetic Spectrometer (AMS; Aguilar et al.,

Final State	Dominant Signals
$W^\pm, Z, \text{gluon, quarks } (u, d, c, s, t, b)$	$p, \bar{p}, D, \bar{D}, e^\pm, \gamma, \nu$
e	e^\pm
μ	e^\pm, ν
τ	e^\pm, γ, ν
γ	γ
ν	ν

Table 1 The first column shows the possible standard model particles that DM could annihilate or decay into. The second column shows the dominant indirect detection signals that arise from these final states. At a smaller level almost every possible signal can be produced by any final state through loop corrections, final state radiation, and inverse-Compton scattering, as discussed in the text.

2002) when finally deployed. Theoretically, each different possible final state can produce a different experimental signature. Even if only two-body final states are counted (particle-antiparticle) this would be 16 possible final states. However, in practice, most of the final states produce similar signatures and are often grouped together when setting experimental limits. So as an approximation it is often sufficient to consider only five types of final states. First, those that contain quarks or the W , Z , or gluon. All these decay through quantum chromodynamical processes, ultimately producing hadrons: p/\bar{p} , and pions (also, possibly D/\bar{D}). The π^0 s decay to gamma rays, while the π^\pm decays produce e^\pm . Second, are final states with e^\pm s or μ^\pm s, which dominantly produce a hard e^\pm spectrum, with the μ^\pm decays also producing ν_μ and ν_e . Third, are final states with τ^\pm . These produce a softer e^\pm spectrum and a strong neutrino signal. In addition, the τ^\pm can decay hadronically to pions (but, never protons) and thus can also produce a strong gamma-ray signal. Fourth, if there is a photon in the final state it produces a strong gamma-ray signal with a hard spectrum and often either a sharp edge, or in the case of a two-body final state, a line in the gamma-ray spectrum. Lastly, final states with neutrinos dominantly produce only a hard neutrino spectrum as they do not decay. This is summarized in table 1. Secondarily, each of these final states can also produce every other type of particle including gamma rays and protons by quantum loop corrections, final state radiation, and inverse-Compton (IC) scattering. However, this is at a much smaller level than the dominant production modes (see, e.g., Arvanitaki et al., 2009, for a consideration of such processes in the context of DM decays).

If only a specific model (e.g., a supersymmetric or an extra-dimensional model) is considered, then the experimental limits on DM annihilation or decay can be derived for the particular final states predicted by that model, according to Equation 3. However, when setting general experimental limits it is preferable to express them for a few representative final states, so that they are as model-independent as possible. For gamma-ray or CR detectors, it is common to consider limits for gamma-ray line, $b\bar{b}$, and $\mu^+\mu^-$ final states. These provide a good approximation to the likely signals (though not for neutrino detectors) from all

the different final states as explained above and in table 1. The $\mu^+\mu^-$ final state is often motivated by models designed to explain the PAMELA (Payload for Anti-Matter Exploration and Light-nuclei Astrophysics) positron fraction data (see Section 3.1) which require a hard positron spectrum without significant antiproton production. Limits on the $b\bar{b}$ final state apply to most supersymmetric models since it is one of the leading tree-level annihilation channels.

Gamma rays that are produced in the DM annihilations or decays are undeflected by magnetic fields and travel to us from anywhere in the Galaxy, and indeed almost anywhere in the visible Universe, effectively indicating the direction to their source. For a DM source of gamma rays in the nearby Universe, the flux from DM annihilation is given by the integral of the DM density-squared along the line of sight from the observer to the source, multiplied by the production spectrum:

$$\phi_\gamma(E, \psi) = J(\psi) \times \Phi_\gamma(E), \quad (4)$$

where E is the gamma-ray energy, ψ is the elongation angle with respect to the center of the source, $\Phi_\gamma(E)$ is given by Equation 3, and the astrophysical factor is

$$J(\psi) = \int_{\text{l.o.s.}} \rho^2(\ell) d\ell \quad (5)$$

where $\rho(\vec{r})$ is the density of DM particles, and the integration is in the direction ψ along the line ℓ . For gamma rays from decaying DM, $\rho^2(\vec{r}) \rightarrow \rho(\vec{r})$ in Equation 5.

Neutrinos interact so weakly that they simply free-stream from anywhere in the visible Universe and indeed may even come from the early Universe, although in that case they are highly red-shifted. But, if a DM source of neutrinos is not significantly red-shifted, Equation 4 also applies for calculating the flux.

However, if the standard model particles resulting from DM annihilation or decays are charged CRs, they do not travel directly to us. Instead, they are transported to the Solar System via scattering on magnetic irregularities in the interstellar medium (ISM) and halo surrounding the Galaxy. Their trajectories are quickly randomized by such processes so that they retain little information about their initial directions. For energies $\gtrsim 10$ GeV, the energy losses of the CR nuclei are strongly suppressed compared to the lighter electrons and positrons. Hence, the main effect on the CR nuclei is from scattering. Particles produced throughout the halo, at distances of tens of kiloparsecs and further, can reach the Solar System. Electrons and positrons, however, are severely affected by IC scattering on the interstellar radiation field (ISRF) and by synchrotron radiation from spiraling in the Galactic magnetic field. If produced with energies $\gtrsim 100$ GeV, they will reach the Solar System only if their origin is within a few kiloparsecs.

Also, CRs from DM annihilation or decay can produce gamma rays during their transport through the ISM. The CR intensities and spectra, together with the target distributions (ISRF, gas, magnetic field) determine the gamma-ray flux distribution. This involves treating the DM distribution as a source of CRs, calculating the distributions and spectra of these CRs in addition to those

from standard astrophysical sources, and the diffuse emissions taking into account the detailed distributions of the gas, ISRF, and magnetic field. This is a more complicated calculation than using Equation 4 and has to be done using a numerical code, such as GALPROP (Strong & Moskalenko, 1998, see also <http://galprop.stanford.edu>), which allows these many details to be treated.

Disentangling the DM signals from astrophysical backgrounds is not straightforward. Spectral information may provide the most powerful discriminator. It is possible to have a significant branching fraction for DM annihilation or decay into monoenergetic photons, giving a distinctive line in the gamma-ray spectrum. But it is more likely that we must rely on the fact that DM annihilation or decay produces a relatively hard (that is, falling with increasing energy slower than the gamma-ray spectrum of a typical astrophysical source) continuum spectrum with a bump or edge near the WIMP mass that is on top of the astrophysical background. Unless there is a very nearby DM source of CRs, spectral information is the only method for distinguishing between a DM signal and astrophysical origin for these particles.

However, for gamma rays and neutrino DM signals spatial information can also be used. We can take advantage of the expected shape of the Galactic DM halo, or it can be used to search for isolated DM subhalo objects, which can appear to be extended objects in the gamma-ray sky if sufficiently large and nearby. But annihilation depends so strongly on the DM spatial distributions at small scales that our uncertainty in them becomes a significant issue. Massive many-body calculations are commonly used to predict the DM distributions on Galactic (e.g., Diemand, Kuhlen & Madau, 2007) and extragalactic scales (e.g., Boylan-Kolchin et al., 2009), but they suffer from two serious limitations. First, the effects of baryons are not fully included, if at all, but in reality baryons must affect significantly the DM distribution in important regions such as the Galactic center (GC). Second, even the purely gravitational DM calculations cannot probe to small scales, due to numerical limitations. So analytic extrapolations are needed to predict behavior in the densest regions, just where the annihilation is most pronounced. The resulting uncertainty is often expressed in terms of a boost factor, which gives the relative increase in overall annihilation rate due to small-scale structure not predicted by the numerical many-body calculation.

1.4 Other Indirect Dark Matter Signals

It is also possible that annihilation of DM trapped within the Sun or the Earth is a significant source of neutrinos. The neutrinos would escape and might be seen in a detector (Silk, Olive & Srednicki, 1985) such as Super-K (Desai et al., 2004) or IceCube (Abbasi et al., 2009, 2010). Such a point source with a hard spectrum would be convincing evidence that the neutrinos originated from DM. DM builds up in the centers of the Earth and Sun when a WIMP traveling through either body collides with a nucleus and loses enough energy to become gravitationally bound. It then orbits the center of the object, undergoing multiple collisions. The neutrino production rate depends on both the DM annihilation cross section and the DM-nucleon scattering cross section. The latter is constrained by di-

rect detection experiments such as CDMS (Ahmed et al., 2010) and XENON100 (Aprile et al., 2010) to be $\lesssim 3 \times 10^{-44} \text{ cm}^2$ for DM masses $\sim 100 \text{ GeV}$.

Recent work (Moskalenko & Wai, 2007; Hooper et al., 2010; McCullough & Fairbarn, 2010) has also brought to light the possibility that DM may be captured inside white dwarf stars at high rates. In fact, in certain circumstances the energy deposited in the star by DM annihilations can dominate its luminosity, providing a constraint on the DM-nucleon scattering cross section. The limit placed so far is fairly high and thus generally constrains only models of DM that somehow avoided the direct detection constraints. It becomes more interesting if the density of DM surrounding the white dwarf is much larger than the local DM density. Although such places may exist, for example in globular clusters, it is difficult to know their actual DM density. Therefore, this limit is uncertain until the DM density can be measured accurately.

There is also evidence from the INTEGRAL/SPI instrument for an anomalously large intensity of the 511-keV positron annihilation line from the central region of the Galaxy (Teegarden et al., 2005). Although this may well have a standard astrophysical explanation, DM has also been postulated as the source. For example, light WIMPs (Hooper & Zurek, 2008) could annihilate to produce positrons, or WIMPs might upscatter to an excited state (Finkbeiner & Weiner, 2007) and then decay to produce the positrons. See the review by Prantzos et al. (2011) for an extensive discussion of possible origins of the 511-keV line.

2 EXPERIMENTS

DM annihilation or decay into standard model particles produces CRs, photons, and neutrinos. CRs and gamma rays have been measured by many experiments, but the detection of high-energy neutrinos from extraterrestrial sources has so far proved elusive.

The experiments dedicated to the study of charged particle CRs range from deep space probes such as NASA's *Advanced Composition Explorer* (ACE; Stone et al., 1998), to orbiting particle detectors such as PAMELA (Picozza et al., 2007), to massive balloon payloads, e.g., BESS (Shikaze et al., 2007), to enormous ground-based arrays such as the Pierre Auger Observatory (Abraham et al., 2004). Gamma-ray instruments also operate in space, such as EGRET (Thompson et al., 1993) on the *Compton Gamma Ray Observatory*, the *Fermi Large Area Telescope* (*Fermi*-LAT; Atwood et al., 2009), and AGILE (Tavani et al., 2008), and on the ground, e.g., the Imaging Air Cherenkov Telescopes (IACTs) High Energy Stereoscopic System (HESS; Hinton, 2004), Major Atmospheric Gamma Imaging Cherenkov telescope (MAGIC; Ferenc et al., 2005), and Very Energetic Radiation Imaging Telescope Array System (VERITAS; Weekes et al., 2002). Meanwhile, IceCube (Halzen & Klein, 2010) is nearing completion and is anticipated to inaugurate the era of neutrino astronomy. Here, we provide a brief history of CR detectors and measurements that have motivated the search for particle DM and discuss in more detail the modern CR, gamma-ray, and neutrino experiments that are directly relevant to astroparticle DM searches.

2.1 Cosmic-Ray Instruments: 1960s to Early 2000s

The first detection of CR antimatter involved positrons (De Shong, Hildebrand & Meyer, 1964). However, it was early measurements of CR antiprotons that inspired models for production by exotic processes. The first measurements of the antiproton/proton ratio as a function of kinetic energy came from balloon-borne experiments in the late 1970s (Golden et al., 1979; Bogomolov et al., 1979). Early calculations for both antiprotons and positrons focused on secondary production by inelastic collisions of CR nuclei with interstellar gas, which is considered to be the standard astrophysical production mode. See, e.g., Shen & Berkey (1968) and Gaisser & Levy (1974) regarding antiprotons and, e.g., Protheroe (1982) and references therein regarding positrons. The kinematics of antiproton production combined with a steeply falling incident CR proton spectrum produce a distinctive spectral shape peaking around ~ 2 GeV. A large excess over the expected astrophysical background at low energies was measured by a balloon-borne detector (Buffington, Schindler & Pennypacker, 1981), which employed a different detection method than the earlier experiments. This stimulated interest in alternative explanations, including the annihilation of DM in the Galactic halo (e.g., Silk & Srednicki, 1984; Stecker, Rudaz & Walsh, 1985; Jungman & Kamionkowski, 1994). Annihilation signatures via other modes, e.g., positrons and gamma rays, were also predicted (e.g., Turner, 1986; Rudaz & Stecker, 1988; Kamionkowski & Turner, 1991).

Background contamination was a serious issue for these early experiments (see Tarlé & Schubnell (2001) and the discussion of Moskalenko et al. (2002) in their Section 4). Later experiments utilizing modern methods for particle identification reduced the upper limits on the low-energy antiproton flux (e.g., Salamon et al., 1990) until finally detection was achieved at a level 40 to 100 times lower than claimed by Buffington, Schindler & Pennypacker (1981). Prior to the launch of PAMELA, balloon-borne instruments employing differing detection methods, such as IMAX (Mitchell et al., 1996), CAPRICE (Boezio et al., 1997, 2001), BESS (Moiseev et al., 1997; Maeno et al., 2001; Asaoka et al., 2002), and HEAT-pbar (Beach et al., 2001) have yielded reliable data on the antiproton spectrum and fraction over the range of ~ 200 MeV to ~ 50 GeV.

Balloon experiments through the 1980s measured CR electrons and positrons with inconsistent results (e.g., Müller & Tang, 1990, and references therein). Some authors interpreted the data $\gtrsim 10$ GeV for the CR positron fraction as evidence for nearby high-energy CR sources (e.g. Aharonian et al., 1995) that provided additional electrons and positrons on top of the standard contribution by CR nuclei colliding with the interstellar gas. (The production spectrum for the secondary positrons and electrons in the ISM follows the parent CR nuclei spectrum, which has a power-law index ~ -2.7 . The primary CR electrons produced in, e.g., supernova remnants, outnumber the secondaries by a factor ~ 10 or more, depending on energy. The primary electrons have source spectra typically flatter than the secondary positrons by $\sim 0.3 - 0.5$ dex. While propagation and energy losses further steepen the spectra, these effects are independent of charge sign, so the positron fraction from this process falls with increasing energy ap-

proximately as the ratio of the source spectra. CR nuclei interacting with gas in the ISM cannot explain a positron fraction that rises with increasing energy.) However, the overwhelmingly large CR proton flux (protons outnumber electrons by a factor ~ 100 at GeV energies) presents a serious impediment to accurate measurement of positrons. The two look nearly identical in a magnetic spectrometer, so additional instruments such as calorimeters and transition radiation detectors must be employed to distinguish them. Because positrons comprise $\lesssim 0.1\%$ of the total CR flux above ~ 1 GeV, to achieve a signal-to-noise ratio better than unity already requires discrimination better than $\sim 10^{-3}$, which is challenging to achieve with controlled systematic errors. Furthermore, because the proton spectrum falls less steeply than the positron spectrum, the required discrimination increases with energy. The early experiments most likely did not achieve the necessary level of background rejection.

The use of modern particle-physics instrumentation on balloons or in orbit steadily advanced the measurement of CR positrons. Starting from the mid-1990s, the HEAT experiment (Barwick et al., 1995, 1997, 1998; Du Vernois et al., 2001; Beatty et al., 2004) and CAPRICE (Barbiellini et al., 1996; Boezio et al., 2000) measured the CR positron spectrum and fraction up to ~ 50 GeV, finding results that were in most respects consistent with standard CR nuclei-ISM secondary production. However, a small excess in the positron fraction above ≈ 7 GeV was detected by HEAT and also seen in CAPRICE data, as well as by the test flight of AMS (Advanced Magnetic Spectrometer) (Aguilar et al., 2002). Several possible origins for this excess were proposed, e.g., DM, pulsars, and CRs interacting with giant molecular clouds (e.g., Couto et al., 1999; Du Vernois et al., 2001). We will discuss this further in Section 3.1.

2.2 Current Cosmic-Ray and Gamma-Ray Experiments

Charged CRs are by far the most numerous of the high-energy particles observed and can be detected over a wide range of energies both by balloon- and space-based instruments, as well as from the ground at sufficiently high energy. Cosmic gamma rays can be viewed only from space over much of the spectrum of interest here, but above about 100 GeV the showers produced by their interactions with the atmosphere can be viewed from the ground via Cherenkov light produced by the relativistic particles. Both space-based and ground-based gamma-ray telescopes must contend with a background of CRs that are more numerous than the gamma rays by factors of 10^4 or more. In practice, ground-based telescopes have achieved the necessary signal-to-background ratio only in small fields of view, thus restricting them to pointed observations. (The Milagro experiment (Atkins et al., 2003) detected gamma rays as well as CR shower products at ground level over a very wide field of view but nevertheless did not achieve sensitivity to localized sources of gamma rays comparable to that of the IACTs.) Here we briefly describe the CR and gamma-ray experiments currently at the forefront of indirect searches for DM.

2.2.1 Balloon-Borne Experiments The Advanced Thin Ionization Calorimeter (ATIC) experiment reported in 2008 a measurement of the high-energy CR electron flux that attracted a lot of attention (see Section 3.1) due to a significant bump in the spectrum around 600 GeV (Chang et al., 2008b). ATIC flew on a high-altitude balloon in two Antarctic circumpolar flights in 2000/2001 and 2002/2003 for a total exposure of $3.08 \text{ m}^2 \text{ sr days}$. (Preliminary data from a third successful flight in 2007/2008 have been shown in conferences to support earlier results, e.g., an unpublished talk by J. P. Wefel at the HEAD 2010 meeting at Waikoloa Village, Hawaii.) The instrument is a calorimeter that was optimized for detection and identification of CR nuclei. It consists of a low-Z (1.2 interaction lengths of carbon) active target, designed to measure the charge magnitude of the incoming CR and to initiate the first interaction, followed by a thick (18 radiation lengths), finely segmented bismuth germanate (BGO) calorimeter (Guzik et al., 2004). While the active target is not ideal for electron identification, the BGO calorimeter does excel at measuring electromagnetic showers, and the ATIC electron-proton separation was extensively studied by simulations and in beam-test data (Chang et al., 2008a). A smaller Antarctic balloon-borne experiment, PPB-BETS, reported an excess in the CR data [Torii et al., unpublished data (arXiv:0809.0760)] similar to that seen by ATIC, although with less statistical significance due to four times smaller exposure.

2.2.2 Space-Based Experiments PAMELA is an orbiting instrument dedicated to CR measurements (Picozza et al., 2007) that was launched in 2006. It consists of a magnetic spectrometer, an anticoincidence system (to veto particles entering through the sides of the spectrometer), a time-of-flight system, an electromagnetic sampling calorimeter of 16.3 radiation lengths thickness, a shower-tail-catcher scintillator, and a neutron detector. Its spectrometer can measure the momentum and charge sign of charged CR particles, with a maximum detectable rigidity (momentum per unit charge) of $800 \text{ GeV}/c$, while the time-of-flight system, calorimeter, and neutron detector serve to identify the particle type. Its acceptance for electrons is small compared to those of ATIC and the *Fermi*-LAT (see below), but it is uniquely able to separate electrons from positrons cleanly up to $270 \text{ GeV } c^{-1}$ momentum by means of the magnetic spectrometer.

NASA's *Fermi*-LAT (Atwood et al., 2009), launched in 2008, is the preeminent gamma-ray telescope in the energy range above $\sim 100 \text{ MeV}$. It is a pair-conversion telescope, like its immediate predecessor EGRET (Thompson et al., 1993) and its much smaller contemporary AGILE (Tavani et al., 2008), launched in 2007. Thirty-six layers of silicon-strip detectors interleaved with tungsten foils (Atwood et al., 2007) pair-convert the gamma rays and track the resulting electrons and positrons. The tracking section is followed by a segmented CsI crystal calorimeter that measures the energy of the electromagnetic shower. A veto-counter system (Moiseev et al., 2007), based on segmented scintillator tiles, helps to tag charged CRs and, together with the detailed event reconstruction in the tracker and calorimeter, reduce that background by at least five orders of magnitude. The tracking resolution is generally limited by multiple scattering of the electrons and

positrons in the tungsten foils and other material, giving a point-spread function (PSF) with 68% containment angles for individual photons ranging from a few degrees at 100 MeV down to about 0.1° for energies $\gtrsim 10$ GeV.

The *Fermi*-LAT has an extraordinarily large field of view of 2.4 sr, thus seeing nearly 20% of the entire sky at any instant. It normally operates pointing outward from the Earth, scanning the sky, and achieves a fairly uniform exposure over 4π sr by rocking back and forth by 50° toward one orbital pole or the other on successive orbits. Its all-sky view together with its excellent signal-to-noise and large energy range, from ~ 100 MeV to beyond 300 GeV, make it very well suited to searches for DM annihilation in all types of possible sources, point-like or diffuse, Galactic or extragalactic.

The *Fermi*-LAT is also a very capable CR electron detector (Ormes & Moiseev, 2007). It has no atmospheric overburden and already has an exposure at least 200 times larger (depending on energy) than that of ATIC. See Section 3.1 for a comparison of the electron results from the two experiments.

2.2.3 Ground-Based Experiments Gamma-ray astronomy with IACTs was pioneered by the *Whipple* telescope (Cawley et al., 1990), which first coupled a pixelated photomultiplier-tube camera to a large (10-m) optical reflector, giving it the ability to image the atmospheric showers and thereby reject much of the CR background. *Whipple* was the first IACT to detect an extragalactic source, Markarian 421, in the TeV energy range (Punch et al., 1992). The four IACTs that dominate the field today are based on the same technique but extend it to arrays of larger reflectors that achieve larger effective areas, lower thresholds, and lower background. The HESS experiment in Namibia (Hinton, 2004) and the VERITAS experiment in Arizona (Weekes et al., 2002) are similar but complement each other by being in opposite hemispheres. Each is an array of four 13-m-diameter IACTs. (An enormous 600 m² reflector will be added to HESS for its second phase.) Another southern-hemisphere instrument is the CANGAROO-III array of four 10-m-diameter IACTs (Kabuki et al., 2003), while a second northern-hemisphere instrument is MAGIC, a pair of 17-m-diameter IACTs located on the Canary Island of La Palma (Ferenc et al., 2005).

IACTs have small fields of view ranging from 3.5° (MAGIC, VERITAS) to 5° (HESS) and therefore most often operate by pointing at known objects. Scans over the sky are time consuming but have been accomplished over limited regions, such as the HESS scan of the inner Galaxy (Aharonian et al., 2006). Their observing time is limited to clear, dark nights with little or no moonlight (less than half full), for a total typically of around 900 hours per year, and their power to reject charged CR background is roughly 100 worse than that of *Fermi*. However, their effective areas are very large (up to 10^5 m² compared with less than ≈ 0.8 m² for *Fermi*-LAT). Their trigger energy thresholds range from about 25 GeV (MAGIC) to 100 GeV (VERITAS), although the threshold for spectral reconstruction is higher (150 GeV for VERITAS), providing some overlap with *Fermi*-LAT for the brightest sources (such as the Crab pulsar wind nebula). In general, IACT energy resolutions are about 15% at high energy, with single-

photon angular resolutions of around 0.1° (similar to the resolution achieved by *Fermi*-LAT above 10 GeV). More details on the IACT method and instruments are available in the review by Hinton & Hoffman (2009).

2.3 Neutrinos

So far, neutrinos from sources outside of the Solar System have not been detected except in the case of a single fortuitous supernova event in the Large Magellanic Cloud, SN1987A, from which neutrinos were detected by two underground experiments (Bionta et al., 1987; Hirata et al., 1987). However, new experiments with very large sensitive volumes are planned or are under construction with the intent to realize the potential of neutrino astronomy (Anchordoqui & Montaruli, 2010).

Only the $> 90\%$ completed IceCube detector (Halzen & Klein, 2010) at the South Pole is currently reaching the cubic-kilometer scale thought to be necessary for the dawn of neutrino astronomy. Neutrinos traveling through the Earth can interact to produce particles traveling upward through the Antarctic ice. Cerenkov light from the relativistic particles is detected by photomultiplier tubes arranged on 80 strings 2,450 m long descending into the ice cap, with the active volume all below a depth of 1,450 m.

IceCube has an irreducible foreground of neutrinos produced in Northern-Hemisphere CR showers. Those are almost all muon neutrinos, so it is advantageous to distinguish electron and tau neutrino events in IceCube from those produced by muon neutrinos, even though the latter give the best directional information. Very high-energy tau leptons can travel hundreds of meters in the detector before decaying, yielding distinctive double-vertex events, whereas electrons and low-energy taus deposit their energy in localized showers, giving excellent energy resolution but little directional information.

The angular resolution for long muon events is about one degree, and the energy threshold is ≈ 100 GeV. Six additional closely spaced strings of detectors lowered into the deepest 350 m of ice will form a “Deep Core” infill array with a significantly lower (10 GeV) threshold. The IceCube detector has been operational even during construction, and neutrino sky maps have been made with a half-year exposure of a 1/2 cubic km detector, yielding nearly 7,000 neutrinos from the Northern Hemisphere (Halzen & Klein, 2010).

3 RECENT DATA AND INTERPRETATIONS

3.1 Cosmic Rays

The PAMELA instrument team has reported measurements of the antiproton spectrum and fraction (Adriani et al., 2009b, 2010b), and the positron fraction (Adriani et al., 2009a, 2010a). Figure 1a shows the combined measurements of the CR antiproton fraction as of late 2010 (Adriani et al., 2010b), whereas Figure 1b shows the CR positron fraction as measured by many experiments up to late 2009 (Adriani et al., 2009a). The PAMELA antiproton measurements agree with

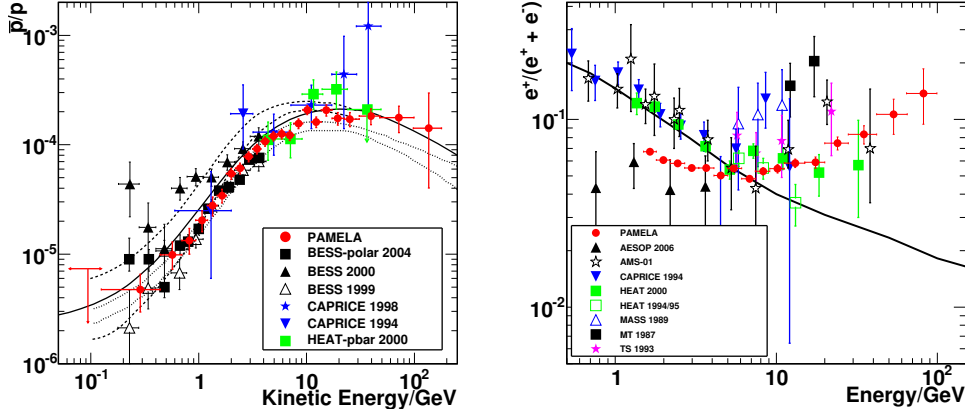


Figure 1 (a) Cosmic-ray (CR) antiproton fraction and (b) positron fraction. The CR measurements by various instruments are summarized in Adriani et al. (2010b) (antiprotons) and Adriani et al. (2009a) (positrons). For antiprotons, the curves correspond to models with different assumptions for the treatment of CR propagation, uncertainties in the assumed propagation model parameters, and cross section uncertainties for antiproton production, annihilation, and scattering. Upper and lower dashed lines were calculated for a homogeneous (leaky box) model by Simon, Molnar & Roesler (1998). Upper and lower dotted lines were calculated assuming a diffusive reacceleration with convection model by Donato et al. (2009). Solid line shows the calculation by Ptuskin et al. (2006) for a plain diffusion model. For positrons, the solid curve shows the prediction by Moskalenko & Strong (1998) using the GALPROP code for CR nuclei interacting with the interstellar gas for a plain diffusion model without accounting for solar modulation effects. Figures are adapted from original forms published in Adriani et al. (2010b) and Adriani et al. (2009a).

earlier data (where there is overlap), which are consistent with expected non-exotic astrophysical origins. However, the PAMELA positron fraction rises with increasing energy, opposite to the expected behavior of secondaries produced in the ISM (see Section 2.1). The PAMELA data apparently confirm the results from the earlier HEAT balloon experiment and AMS test-flight (although the results of both of those experiments have much larger uncertainties).

An essential question for these data is the likelihood that they are the result of an experimental artifact. (Recall, in Section 2.1 we discussed how reliable proton-positron discrimination is essential for this measurement.) PAMELA uses its magnetic spectrometer, time-of-flight system (at low energy), calorimeter, and neutron detector for the separation of protons and antiprotons from positrons and electrons (see Section 2.2.2). The spectrometer separates the electrons and antiprotons from the positrons and protons (except at the highest energies, where there is some spill-over; Adriani et al., 2010a). The calorimeter is able to separate electromagnetic- and hadron-initiated (proton/antiproton) showers very well using information on the longitudinal and lateral shower development. However, early neutral pion production at the top of the calorimeter by interacting hadrons produces an electromagnetic shower in hadron-initiated events at about

the percent level. This makes the separation between true electromagnetic- and hadron-initiated events difficult when this occurs because the two look essentially identical in the calorimeter. For the protons and positrons, because the ratio of these particles is large (in favor of the protons) and rises with energy, a slightly larger than expected misidentification of protons could easily lead to a rising positron fraction. The PAMELA collaboration has published details of their analysis, including performance of the particle discrimination (Adriani et al., 2010a). However, some researchers have questioned if sufficient rejection power is obtained by the instrument (Schubnell, 2009) because additional hadron/electromagnetic discrimination systems, like transition radiation detectors, are not used. It would be useful to have the absolute positron spectrum that PAMELA measures to ascertain whether anomalous spectral features also exist in that, but so far it has not been published. These questions will be resolved by follow-up measurements by the AMS experiment, which is due for deployment on the International Space Station in early 2011. AMS will employ multiple systems, such as calorimeters and transition radiation detectors, to separate protons and positrons (Carosi, 2004). It will also separate electrons from positrons to higher energy and will have a much larger acceptance than PAMELA.

Recent measurements of the total CR electron spectrum have also shown anomalies. (We use ‘electron’ here to mean both electrons and positrons, since the ATIC and *Fermi*-LAT instruments are not able to discriminate particles on the basis of charge. When we need to distinguish between electrons and their anti-particle, we explicitly refer to the latter as positrons.) Toward the end of 2008 the ATIC collaboration (Chang et al., 2008b) announced a surprising result: a bump in the CR electron spectrum in the energy range $\sim 300 - 800$ GeV, where conventional astrophysical sources are expected to produce a smooth, power-law spectrum. The PPS-BETS experiment [Torii et al., unpublished data (arXiv:0809.0760)] detected a similar excess over approximately the same energy range as ATIC, although with less statistical significance. See Figure 2 for the combined measurements of the CR electron spectrum up to the end of 2010. Together with the positron fraction measured by PAMELA, these results stimulated a lot of speculation about the origin of the spectral features: DM, certainly, but also that the assumptions for the distribution of astrophysical CR sources and propagation were too simplistic. [This has been suggested since the late 1960s but the measurements until those recently by the *Fermi*-LAT have suffered from large uncertainties at high energies, where the usual assumptions break down. Even with the significantly improved measurements it is still difficult to make strong conclusions about the origin(s) of the CR electrons measured above a few hundred GeV. We discuss this further below.]

However, as Figure 2 shows, the measurement by the *Fermi*-LAT of the CR electron spectrum from 20 GeV to 1 TeV (Abdo et al., 2009b) smoothly connects with the HESS electron measurements at higher energies (Aharonian et al., 2008b, 2009d). The *Fermi*-LAT measurement does not show the anomalous spectral features described by ATIC and PPB-BETS. Extensive details of the *Fermi*-LAT analysis were provided in a follow-up publication (Ackermann et al., 2010c), which

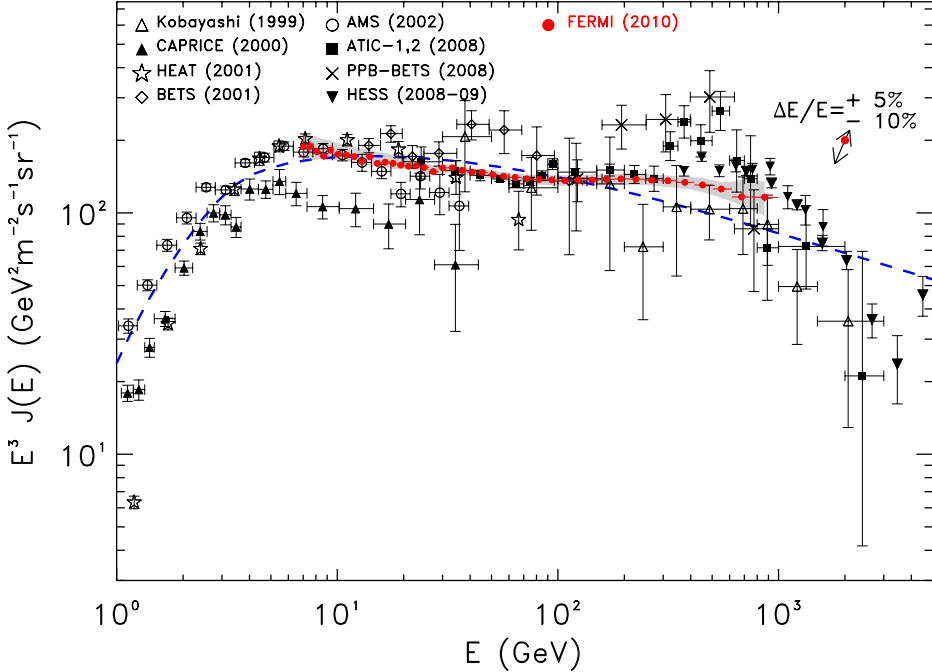


Figure 2 Combined cosmic-ray (CR) electron and positron spectrum as measured by *Fermi*-LAT from ~ 7 GeV to 1 TeV for one year of observations, together with other measurements (Abdo et al., 2009b; Ackermann et al., 2010c, and references therein). The systematic errors for the *Fermi*-LAT measurement are shown by the grey band. The systematic uncertainty associated with the absolute energy scale is shown by the non-vertical arrow in the upper right corner of the figure. (The arrow shows the rigid shift of the entire spectrum due to the uncertainty in the energy scale that takes into account multiplying the spectrum by E^3 .) The dashed line shows the predicted total CR electron and positron spectrum for a diffusive-reacceleration CR propagation model based on CRs and other data measured prior to the *Fermi*-LAT results (Abdo et al., 2009b). This model was not tuned to the *Fermi*-LAT measurements and used a CR electron injection spectrum that was a single power law above ~ 100 GeV. The figure clearly illustrates that the data are not well-reproduced by such a simple spectral model. Possible explanations are discussed in the text, the most likely being that the underlying assumptions commonly used to treat astrophysical CR sources and propagation are too simplistic.

also extended the previous measurements down to the geomagnetic cut-off energy for the *Fermi*-LAT orbit (~ 7 GeV). Detailed simulations of the *Fermi*-LAT instrument and comparison with beam-test data demonstrated that the energy resolution was more than adequate to see a spectral feature like the ATIC peak. Because of the large statistics for the *Fermi*-LAT CR electron data (over 8 million electron candidate events for the first 12 months of the mission) it was possible to apply more stringent cuts on subsets of the data to cross check the full analysis. An analysis was done for a subset of events using only tracks passing through

at least 12 radiation lengths of calorimeter (16 radiation lengths on average), which found consistent results with the analysis of the full event sample. This conclusively ruled out the possibility that any ATIC-like feature was missed in the earlier Abdo et al. (2009b) analysis.

Nevertheless, there is a less dramatic feature apparent above ~ 200 GeV in the *Fermi*-LAT spectrum. Its significance is hard to estimate, due to the existence of both correlated and uncorrelated (from energy bin to energy bin) systematic uncertainties in the instrument acceptance. Separating the two types of uncertainties is a difficult problem that so far has not been accomplished by the *Fermi*-LAT team. While the data are compatible with a power-law spectrum within the displayed band of systematic uncertainties, if a model with a power-law spectrum that is constrained by other data (such as the model curve shown in Figure 2) is compared with the *Fermi*-LAT spectrum, then the significance of the spectral feature above ~ 200 GeV can be very high. Therefore, the *Fermi*-LAT data and the rising positron fraction measured by PAMELA have motivated the construction of DM models to reproduce the apparent features observed by these instruments.

Because DM annihilation or decay creates equal amounts of matter and antimatter with a hard spectrum up to the DM particle mass [$\mathcal{O}(100\text{ GeV})$], it can naturally produce a rising positron fraction and has been a widely conjectured explanation of the PAMELA positron data. However, models must also explain several unexpected characteristics of these data. The relatively large number of additional electrons and positrons produced requires a self-annihilation cross section $\sim 10^2$ to 10^3 times larger than given by Equation 2 (see Figure 6, also). In addition, the measured antiproton fraction does not rise with energy (see Figure 1a), which requires hadron production to be suppressed. Because such a large enhancement of the cross section cannot be simply ascribed to uncertainty in the spatial distribution of the DM (the boost factor; see Section 1.3) several kinds of non-standard DM models have been developed to fit both the PAMELA and *Fermi*-LAT data. (The *Fermi*-LAT data provide an upper bound to enhancements in the cross section.) These include adding a Sommerfeld enhancement to the cross section due to a hypothetical long-range force (e.g., Arkani-Hamed et al., 2009), a nonthermal production mechanism (e.g., Nelson & Spitzer, 2010; Fairbairn & Zupan, 2008), or DM decay (e.g., Arvanitaki et al., 2009).

A more likely explanation of these CR data is that the assumptions made estimating the astrophysical background are overly simplified. Any DM signal in CRs exists on a background of particles from astrophysical sources (e.g., supernovae, supernova remnants, pulsars, compact objects in close binary systems, stellar winds, etc.). The primary CRs, mostly nuclei, are produced at their sources, eventually escaping to propagate in the ISM of the Galaxy, where their spectra change over tens of millions of years as they lose or gain energy through interactions with the interstellar gas, ISRF, magnetic fields and turbulence. Their composition also changes as the destruction of primary CR nuclei via spallation on the interstellar gas gives rise to secondary particles, including nuclear isotopes that are rare in nature, antiprotons, and electrons, positrons, and neutrinos from

the decays of charged pions. Within the Solar System, charged CRs with energies below a few tens of GeV energies are affected by the solar wind. This solar modulation alters the interstellar spectra to produce what we observe locally. Our understanding of CR sources and propagation, the distributions of the target distributions in the ISM (interstellar gas, ISRF, magnetic field), and the heliospheric transport of CRs all impact our ability to disentangle DM from astrophysical signals.

For modeling CR production from astrophysical sources, the assumption is usually made that the sources are described by a smoothly varying function of position, and that they have a common characteristic source spectrum. The assumed spatial distribution is typically based on supernova remnant and pulsar surveys (e.g., Case & Bhattacharya, 1998; Lorimer et al., 2006). That is an acceptable approximation for CR nuclei, barring errors in the data-derived distributions, which are influenced by selection effects. However, for CR electrons and positrons the severe radiative losses from interactions with the ISRF and interstellar magnetic field mean that a source of high-energy electrons must be within ~ 1 kpc if the detected particles are to have energies larger than a few hundred GeV (e.g., Berkey & Shen, 1969; Shen, 1970; Atoyan, Aharonian & Völk, 1995, see also Section 1.3). Therefore, assuming a smooth spatial distribution is not correct, and details of the discrete source distribution in the vicinity of the Solar System are important. Many authors also assume that the ISM is homogeneous, which is incorrect for these particles. [This is typically done for analytic treatments of the CR propagation, since it is not possible to treat arbitrary spatial distributions for the ISM components that determine the energy losses. Even at the highest Galactic CR energies ($\gtrsim 100$ TeV), where the dominant electron/positron energy losses are IC scattering of the CMB and synchrotron radiation, inhomogeneities in the magnetic field are important.] Furthermore, the assumption of a single source spectrum is unrealistic, because there are a variety of production mechanisms for high-energy electrons and positrons: acceleration at shocks (e.g., Lagage & Cesarsky, 1983; Hillas, 2005) (electrons only), production of secondary electrons/positrons *in situ* by shock accelerated hadrons (e.g., Blasi, 2009), pair production via different mechanisms (e.g., Aharonian & Atoyan, 1991; Chi, Cheng & Young, 1996), in addition to possible production by DM annihilation or decay.

Although there is no theory of CR propagation based on first principles, the phenomenological description provided by isotropic diffusion models (diffusion-convection, diffusive-reacceleration, etc.) has proven very successful in describing a wide range of CR data: stable secondary nuclei, radioactive nuclei, electrons, and so forth (e.g., Strong, Moskalenko & Ptuskin, 2007, and references therein). In these models, the propagation parameters and boundary conditions are obtained from fits to the CR nuclei data for the secondary-to-primary ratios (e.g., ${}^5\text{B}/{}^6\text{C}$ and $[{}^{21}\text{Sc}+{}^{22}\text{Ti}+{}^{23}\text{V}]/{}^{26}\text{Fe}$), and radioactive abundances (e.g., ${}^4\text{Be}$, ${}^{26}\text{Al}$, ${}^{36}\text{Cl}$, and ${}^{54}\text{Mn}$). Correcting for solar modulation is typically done using the force-field approximation (Gleeson & Axford, 1968) that uses a single parameter, the modulation potential, to characterize the strength of the effect. Direct

comparison between propagation model calculations and data is problematic because the modulation potentials from different experiments cannot be interpreted independently from the experiments. The derived values depend on the choices of interstellar spectra used for their analyses, which differ from experiment to experiment (and are sometimes not provided). Coupled with the uncertainties in the propagation model, cross sections, and other details, finding a unique set of parameters to describe the CR nuclei data is challenging, which also affects the predictions for CR leptons. Some recent work illustrates their effect for predictions of CR positron spectra using analytic propagation model solutions (e.g., Delahaye et al., 2009). So far, a systematic exploration using a numerical code such as GALPROP has not been performed.

A more subtle issue is related to the treatment of the inhomogeneous CR electron source distribution within a particular propagation model. To our knowledge, a self-consistent calculation deriving the propagation model parameters from the CR nuclei data, and including the discrete electron/positron sources while taking into account the inhomogeneous energy losses, has not been accomplished. Researchers commonly use the free-space 3-dimensional spherically symmetric analytic diffusion results of Aharonian et al. (1995) to treat the nearby source contribution and then a diffusion model variant (either numerical or analytically solved) with a smooth spatial distribution for the far ($\gtrsim 1$ kpc) sources (it is reasonable to assume a smooth spatial distribution for these because the propagation and energy losses erase any details related to the discrete distribution). The problem is that the propagation parameters used to calculate the nearby contribution are obtained from the propagation model used for the far sources [which may not have the same spatial configuration (2/3-dimensional cylindrical/cartesian), boundary conditions, and/or distributions for ISM components], or simply adopted from the literature. This inconsistent treatment of the sources and propagation by essentially all calculations done so far clouds the interpretation of their results.

Given the uncertainties associated with modeling the CR sources, propagation, and so forth, we believe that it is highly plausible that both the PAMELA data and the total electron spectrum can be explained by modifying the assumptions usually made when calculating the standard astrophysical background. For example, the electron and positron data have been explained in terms of contributions from the nearest known pulsars and supernova remnants (e.g., Cowsik & Lee, 1979; Kobayashi et al., 2004, and many other papers). But we emphasize that even for these calculations there is no unique set of sources that have been identified to explain the measured data. In these models, the injected CR power by each source is unknown and is treated as a free parameter that is adjusted to reproduce the observations. Depending on the assumed production mode for the CRs there are some restrictions on inhomogeneous models, and care must be taken not to violate other observational constraints. For example, *in situ* production of secondary electrons and positrons also produces more antiprotons and secondary nuclei if CR nuclei are accelerated together with protons (Lagage & Cesarsky, 1985), which can be inconsistent with other measurements (but, again,

such models have additional adjustable parameters, e.g., the amount of matter in the CR confinement region at the source, which directly affects the total number of secondaries produced and injected into the ISM). Or for pair production on soft photon fields (e.g., Stawarz, Petrosian & Blandford, 2010), intensities for the ISRF much higher than observed are needed in order to produce the required numbers of additional positrons. In short, despite being apparently viable explanations of the CR data, none of the non-exotic models can be pointed to as the unique solution. Thus the DM explanations, although not essential, also remain viable.

3.2 Galactic Diffuse Emission

The diffuse non-thermal emission of photons from radio to gamma-rays is closely connected to the production and propagation of CRs. In inelastic collisions with the interstellar gas, CR nuclei produce neutral pions, which decay to gamma rays. Primary CR electrons and secondary electrons and positrons produce gamma rays via bremsstrahlung with the interstellar gas and by IC scattering off of the ISRF. They also produce diffuse emission in the radio to microwave band by synchrotron radiation induced by the Galactic magnetic field. Because gamma rays are not deflected by magnetic fields, and because their absorption in the ISM is negligible over Galactic distances up to energies of $\sim 10^5$ GeV (Moskalenko, Porter & Strong, 2006), they directly probe CR spectra and intensities in distant locations (see Moskalenko, Strong & Reimer (2004) and Strong, Moskalenko & Ptuskin (2007) for reviews). Here we discuss only the diffuse emission of the Milky Way, for which we have the best data and which are most relevant to constraining the contributions from DM.

The EGRET “GeV excess” was an anomalous signal in the diffuse Galactic emission observed in EGRET data. The term referred to emission for gamma-ray energies $\gtrsim 1$ GeV that was in excess of diffuse gamma-ray emission models based on locally measured CR spectra (see, e.g., Figure 7 of Hunter et al., 1997). It was proposed that the GeV excess was due to gamma rays from annihilating DM (de Boer et al., 2005a,b). This received much attention, but a number of more conventional or prosaic explanations were also considered, e.g., variations in the CR spectra (Porter & Protheroe, 1997; Strong, Moskalenko & Reimer, 2000, 2004b) and hypothesized instrumental effects (Hunter et al., 1997). The DM interpretation was itself challenged because the DM models employed over-produced antiprotons relative to the data already available (Bergström et al., 2006).

Testing the origin of the GeV excess was one of the early studies of the diffuse gamma-ray emission by the *Fermi*-LAT team (Abdo et al., 2009d). The data at intermediate Galactic latitudes ($10^\circ \leq |b| \leq 20^\circ$) were used in the study because the standard astrophysical production of the diffuse gamma-ray emission over this region of the sky come predominantly from relatively nearby CR nuclei interactions with interstellar gas. The majority of the gas is in the form of atomic hydrogen (H I) and molecular hydrogen (H₂), along with a small amount of ionized hydrogen. The H I has roughly uniform density at ~ 1 atom cm⁻³,

with a typical scale height about the Galactic mid-plane of ~ 200 pc (Dickey & Lockman, 1990; Kalberla & Kerp, 2009). The H_2 is concentrated mainly in clouds of density typically $\sim 10^{3-4}$ molecules cm^{-3} and mass 10^{4-6} M_\odot , with a scale height of ~ 70 pc (Combes, 1991). For these latitudes, the CRs producing the majority of the diffuse emission are therefore several hundreds of parsecs to ~ 1 kpc from the Sun. Because the CRs are mainly nuclei, for which energy losses are slow, the CR intensities and spectra are expected to be close to those measured locally. Significant spectral anomalies like the GeV excess would then stand out against the standard astrophysical signal, because this region of the sky avoids the more model-dependent complications inherent in understanding the emission closer to the Galactic plane or at higher latitudes.

The diffuse gamma-ray emission spectra measured by the *Fermi*-LAT and EGRET are shown in Figure 3a, where no attempt has been made to remove the contributions of gamma-ray point sources. The *Fermi*-LAT measured spectrum is significantly softer than that of EGRET. The specific cause of the differences in the spectra measured by these instruments is uncertain. The confidence in the *Fermi*-LAT instrument response comes from detailed Monte Carlo simulations that were validated with beam tests of a calibration units, as well as post-launch refinements based on actual on-orbit particle background measurements. On-orbit studies of the Vela pulsar (Abdo et al., 2009a, 2010e) showed similar deviations between the *Fermi*-LAT and EGRET spectra, so it is unlikely that the difference is due to differing residual particle background contamination.

Figure 3b replots the *Fermi*-LAT data along with the spectra of a diffuse emission model that is based on local CR measurements, sources with $> 5\sigma$ significance measured in the first three months of data, and an unidentified isotropic background component comprised of residual particle contamination, unresolved sources, and unaccounted diffuse Galactic gamma-ray emission, as well as true extragalactic diffuse emission. It was obtained by fitting to data at higher latitudes while holding the model constant. Although the *Fermi*-LAT spectral shape is consistent with the model, the overall emission in the model is systematically low by $\sim 10 - 20\%$. The diffuse gamma-ray emission model is *a priori*, based on local CR measurements taken before the *Fermi*-LAT launch and on other information (e.g., the conversion between CO line intensity and H_2 column density in the ISM, X_{CO}). These uncertainties are not included in the systematic uncertainty band shown in Figure 3b. However, they would only shift the overall intensity higher and would not change the spectral shape (which comes mainly from the CR proton spectrum, measured with fairly good accuracy to be a power law with index ~ -2.7). The close correspondence between the *Fermi*-LAT data and our expectations based on local CR measurements and astrophysical gamma-ray emission processes suggests that the EGRET GeV excess was the result of instrumental errors. In fact, members of the EGRET team have called into question the calibration of their instrument as an explanation of the GeV excess (Stecker, Hunter & Kniffen, 2008), but they did not identify a specific cause.

There have been other claims for the detection of excess diffuse emission (over the standard astrophysical background) at microwave frequencies and gamma-ray

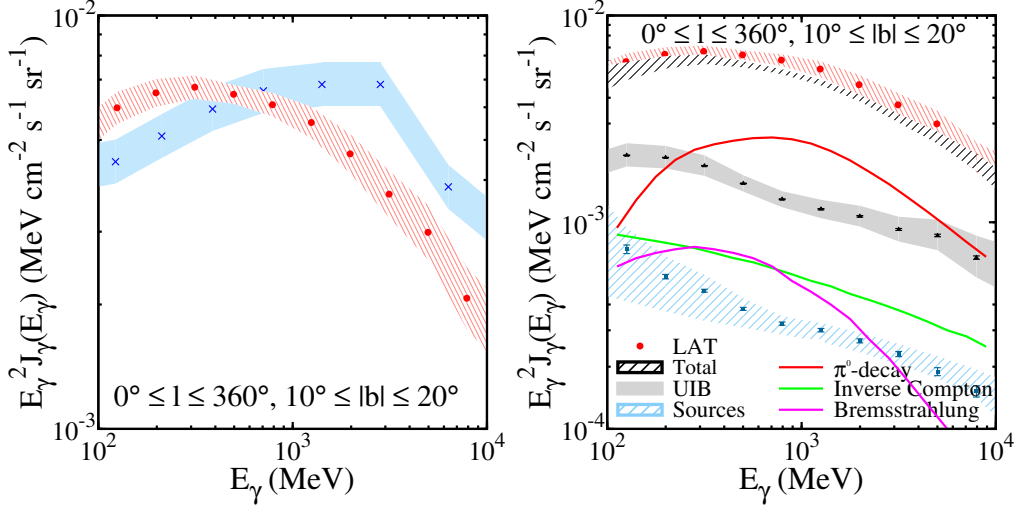


Figure 3 Diffuse gamma-ray emission intensity from 100 MeV to 10 GeV averaged over all Galactic longitudes for the latitude range $10^\circ \leq |b| \leq 20^\circ$ from Abdo et al. (2009d). (a): *Fermi*-LAT (red dots) and EGRET (blue crosses) data. The hatched band surrounding the *Fermi*-LAT data indicates the systematic uncertainty in the measurement due to the uncertainty in the instrument acceptance. The EGRET data have the standard 13% systematic uncertainty (Esposito et al., 1999). The *Fermi*-LAT spectrum is significantly softer than the EGRET spectrum with an integrated intensity $J_{\text{LAT}}(\geq 1 \text{ GeV}) = 2.35 \pm 0.01 \times 10^{-6} \text{ cm}^{-2} \text{ s}^{-1} \text{ sr}^{-1}$ compared to the EGRET integrated intensity $J_{\text{EGRET}}(\geq 1 \text{ GeV}) = 3.16 \pm 0.05 \times 10^{-6} \text{ cm}^{-2} \text{ s}^{-1} \text{ sr}^{-1}$, where the errors are statistical only. (b): *Fermi*-LAT data with components from a diffuse gamma-ray emission model, sources, and unidentified isotropic background (UIB). Model (lines): π^0 -decay, red; bremsstrahlung, magenta; inverse Compton, green. Shaded/hatched regions: UIB (unidentified background), gray shading; sources, blue hatching; total (model + UIB + source), black hatching. The UIB component was determined by fitting the data and sources with the model held constant using the latitude range of $|b| \geq 30^\circ$, and is a measure of the instrumental background due to charged CRs interacting in the LAT, unresolved sources, and unaccounted diffuse Galactic gamma-ray emission components, as well as the true diffuse extragalactic gamma-ray background. The spectral shape of the *Fermi*-LAT data is compatible with the total of the assumed model, sources, and UIB component. No excess emission component is required. Note that the model is *a priori*, based on directly measured CR spectra, and is not fitted to the gamma-ray data. Thus the uncertainty in the total does not reflect any uncertainties associated with modeling the diffuse gamma-ray emission (which are estimated to be $\sim 20\%$ for the selected region of sky in Abdo et al., 2009d).

energies. At GHz frequencies, analysis of the Wilkinson Microwave Anisotropy Probe (WMAP) data showed evidence for excess diffuse emission within a 20° radial region about the center of the Milky Way, which was called the WMAP haze (Finkbeiner, 2004). It is diffuse emission in excess of that expected from dust, ionized gas, and synchrotron radiation by CR electrons, and it has been interpreted as evidence for an additional source of CR electrons and positrons in the inner Galaxy, possibly due to DM annihilation or decay (Hooper, Finkbeiner & Dobler, 2007). Further analysis of 3-year (Dobler & Finkbeiner, 2008; Bottino, Banday & Maino, 2008) and 5-year WMAP data (Bottino, Banday & Maino, 2010) also showed evidence of the excess emission, but analysis of the 7-year WMAP data (Gold et al., 2010) does not show evidence for a polarized signal, casting doubt on a synchrotron-radiation origin of the additional component.

Similarly, analysis of *Fermi*-LAT data has led to claims of a corresponding gamma-ray haze, described as the high-energy counterpart to the WMAP haze (Dobler et al., 2010) and produced by IC scattering of electrons and positrons on the ISRF. Whether or not the WMAP and gamma-ray haze are related is difficult to tell. Furthermore, we should first convince ourselves that the data really are in excess over the expected standard astrophysical sources of diffuse emission.

The analyses of the WMAP and *Fermi*-LAT data by these authors use various fitting methods that employ templates as proxies for the interstellar emission components comprising the astrophysical background, e.g., dust maps and radio data (representing the synchrotron emission) for the WMAP haze, or gas maps and other templates to represent the various diffuse emission components for the gamma-ray haze. The background is removed by some procedure, and the remaining residuals are interpreted as these excess emission components (the WMAP haze or gamma-ray haze). Sometimes the accuracy of the templates representing the spatial morphology over the full frequency (energy) range is debatable. As an example, typically for the analysis of the WMAP data, researchers use the 408 MHz map of Haslam et al. (1982), scaling with a single spectral index up to WMAP frequencies. However, studies show that there is a range of spectral indices (from 2.3 to 3.0) between 408 and 1420 MHz (Reich & Reich, 1988). So it seems unlikely, given the large difference between the frequencies where these surveys were made and the $\sim 20 - 90$ GHz WMAP range, that scaling by a single index is an adequate description for this foreground component. The residuals extracted can be affected by these details. For example, Bottino, Banday & Maino (2008) showed how the morphology of the extracted anomalous GHz emission from the WMAP data is less extended compared to using the standard synchrotron template when using a template based on the difference between K and $K\alpha$ WMAP data.

Similar care is also required with the gamma-ray data, for which details related to the gas tracers and how the IC emission is determined are important. It is known that 21-cm and CO surveys are incomplete tracers of the interstellar gas (e.g., Grenier, Casandjian & Terrier, 2005). An auxiliary gas tracer, like a dust reddening map, needs to be used to account for neutral gas not detected in 21-cm or CO observations (e.g., Abdo et al., 2010a; Ackermann et al., 2010d).

Otherwise spurious sources and extended morphological features appear as residuals simply because of our incomplete knowledge of the total gas column density. But correcting the gas column densities with dust maps is only useful for regions where the dust optical depth is not too high (outside the Galactic plane).

The IC templates are obtained from runs of the GALPROP code (<http://galprop.stanford.edu>) using a model for the ISRF that has uncertainties, particularly in the inner Galaxy, that have not been completely quantified (Porter & Strong, 2005; Porter et al., 2008). A model is used to generate them because there is no observational tracer for this diffuse gamma-ray emission component. The astrophysical IC emission has a smoothly varying and extended spatial morphology that changes depending on the assumptions made for the underlying GALPROP run (and ISRF model) employed to calculate the template used for an analysis. However, DM-induced gamma-ray emission can also have a smoothly varying and extended morphology, because the DM provides an additional source of CR electrons and positrons that can IC scatter the ISRF. Disentangling the effect of incomplete knowledge of the astrophysical emission and potential signal component(s) is difficult when features may be introduced into the residuals due to uncertainties in the background model templates.

Another way to search for residual emission is through direct use of physical modeling codes, such as GALPROP. Exploration for the origin of the WMAP haze and the excess gamma-ray emission, including whether they are related, has been done using GALPROP by several groups (e.g. Lin, Finkbeiner & Dobler, 2010; Linden & Profumo, 2010; Mertsch & Sarkar, 2010). The conclusions are mixed. Either the excesses can be attributed to uncertainties in the modeling (e.g., Linden & Profumo, 2010; Mertsch & Sarkar, 2010), or other components are required that could have either astrophysical or DM origins (e.g., Lin, Finkbeiner & Dobler, 2010; Meng, Slatyer & Finkbeiner, 2010). However, these models involve a decomposition of H I and CO gas maps into galactocentric rings to represent the distribution of interstellar gas, together with other details such as assumed distributions for the CR sources, uncertainties associated with the ISRF (as discussed above), and unresolved point source populations (see, e.g., Strong, 2007). For the WMAP haze the uncertainties in the Galactic magnetic field remain important.

With physical models parameter scans can be made to quantify the systematic uncertainties. An example of an analysis involving a subset of model parameters using the gamma-ray data and GALPROP code is the *Fermi*-LAT team analysis of the isotropic gamma-ray background (see table 1 in Abdo et al., 2010d). It was restricted to Galactic latitudes $|b| \geq 10^\circ$ and investigated the systematic uncertainties associated with the local gas distribution and IC contribution when modeling the Galactic diffuse gamma-ray emission as a foreground to the isotropic gamma-ray emission. The residuals had characteristics similar to the gamma-ray haze found by Dobler et al. (2010) (for the regions of sky common to both analyses), but the morphology changed non-linearly under variation of the model parameters, such that the effects of individual parameters were not easily separable. Thus the residuals and their morphological changes were ascribed to

systematic uncertainties in the foreground modeling for the Abdo et al. (2010d) analysis, without identification of any single model parameter as being the cause.

Recent work with Bayesian methods and the GALPROP code has focused on obtaining constraints for the parameters of diffusive-reacceleration CR propagation models using CR nuclei data (Trotta et al., 2010). The results are consistent with earlier less rigorous analyses, but Trotta et al. (2010) also provide statistically well-motivated uncertainties for the model parameters. In the future such studies can be extended to full parameter scans, including the diffuse emission and other CR data, such as antiprotons and positrons. This would enable a better understanding, on a firmer statistical foundation, of the uncertainties involved when modeling CRs and diffuse Galactic emission. Meanwhile, although the WMAP haze and gamma-ray excesses are interesting and motivate alternative physical explanations of their origin, we think that it is premature to draw conclusions on whether DM is needed or more prosaic explanations are sufficient.

Although the *Fermi*-LAT data convincingly rule out the EGRET large GeV excess, there still is much interest in looking for a smaller excess in diffuse gamma-ray emission from the Galactic halo. Unfortunately, the same issues as discussed at length above in relation to the WMAP and gamma-ray haze also affect the halo analyses. Whether a tool like GALPROP is used to predict the background emission or templates are used, in either case it is difficult to quantify the modeling uncertainties. These issues have thus far prevented the *Fermi*-LAT collaboration from publishing limits on DM annihilation in the Galactic halo based on their all-sky diffuse emission data. The same issues are also critical for interpretation of gamma-ray data for the very innermost regions toward the GC, because the unfolding in this region of the sky depends strongly on the uncertainties associated with distributions of the sources of diffuse emission, not to mention a potentially large number of point sources.

In summary, the diffuse emission from the Galaxy provides the highest statistical power for searching for DM signals. But the challenges in understanding the astrophysical backgrounds are also high and require significant further work before strong conclusions can be made.

3.3 Extragalactic Diffuse Emission

The diffuse Galactic emission presents a strong foreground signal to the much fainter diffuse extra-galactic emission, which is often referred to as the extragalactic gamma-ray background (EGB) and generally assumed to have an isotropic or nearly isotropic distribution on the sky. The EGB was first detected against the much brighter diffuse Galactic emission by the *Small Astronomy Satellite 2* (SAS-2) satellite (Fichtel et al., 1975) and later confirmed by analysis of EGRET data (Sreekumar et al., 1998). The EGB is composed of contributions from unresolved extragalactic sources as well as truly diffuse emission processes, such as possible signatures of large-scale structure formation (Waxman & Loeb, 2000), emission produced by the interactions of ultra-high-energy CRs with relic photons (Kalashev et al., 2009), the annihilation or decay of DM, and many other processes (e.g., Dermer, 2007, and references therein). However, diffuse gamma-

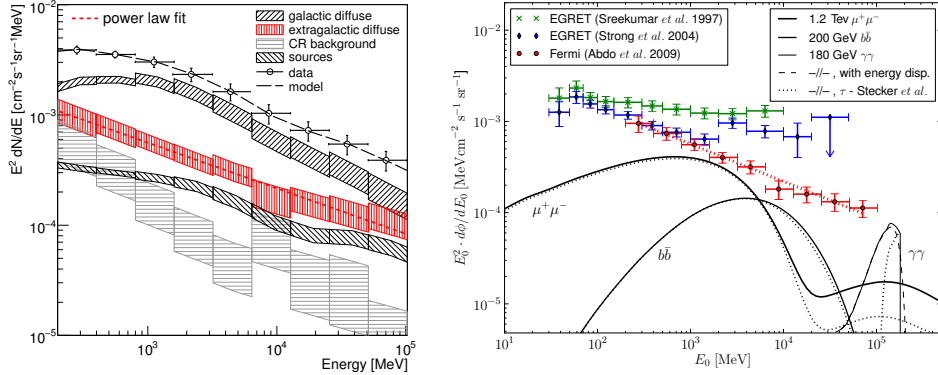


Figure 4 (a) *Fermi*-LAT measured gamma-ray intensity with fit results for the energy range 100 MeV to 100 GeV and averaged over all Galactic longitudes for $|b| \geq 10^\circ$. Fit results by component are given in table 1 of Abdo et al. (2010d). Note that the statistical errors for the *Fermi*-LAT data are smaller than the data symbols, and the systematic uncertainties from the instrument effective area dominate the LAT data for the energy range shown in the figure. The *Fermi*-LAT-derived spectrum for the extragalactic gamma-ray background (shown as the red shaded region) is compatible with a simple power law with index $\gamma = 2.41 \pm 0.05$ and intensity $I(> 100 \text{ MeV}) = (1.03 \pm 0.17) \times 10^{-5} \text{ cm}^{-2} \text{ s}^{-1} \text{ sr}^{-1}$. (b) Extragalactic gamma-ray background spectra derived from *Fermi*-LAT data (Abdo et al., 2010d) and EGRET data [taken from table 1 of Sreekumar et al. (1998) and table 3 of Strong, Moskalenko & Reimer (2004a)], together with three potential types of gamma-ray spectra induced by dark matter (DM) considered in the analysis by Abdo et al. (2010f) (these spectra are good approximations for the likely signals from the different final states discussed in section 1.3 and summarized in table 1). The overall normalization of the DM spectra are obtained assuming a particular extrapolation method for the structure and sub-structure contribution to the DM signal from the Millennium-II numerical calculation (Boylan-Kolchin et al., 2009) [the most conservative scenario considered for the evolution of structure in Abdo et al. (2010f)]. The limits for the annihilation cross sections for the different models are $1.2 \times 10^{-23} \text{ cm}^3 \text{ s}^{-1}$ (for a 1.2 TeV WIMP annihilating to $\mu^+ \mu^-$), $\langle \sigma v \rangle = 5 \times 10^{-25} \text{ cm}^3 \text{ s}^{-1}$ (for a 200 GeV WIMP annihilating to $b\bar{b}$), and $2.5 \times 10^{-26} \text{ cm}^3 \text{ s}^{-1}$ (for 180 GeV WIMP annihilating to $\gamma\gamma$). The solid lines in the figure correspond to the various DM spectra, including the effects of gamma-gamma absorption on the extragalactic background light (EBL) using the model of Gilmore et al. (2009). The dotted lines show the DM spectra, including the effects of gamma-gamma absorption on the EBL using the model of Stecker, Malkan & Scully (2006). The dashed lines are the DM model spectra, including the finite energy resolution of the *Fermi*-LAT for the Gilmore et al. (2009) EBL model. For the $b\bar{b}$ and $\mu^+ \mu^-$ final states, the limits are 10 – 1000 times higher than the cross section given by Equation 2 [limits for the DM models with relatively strong gamma-ray lines are below the current sensitivity of the *Fermi*-LAT (see Abdo et al., 2010f, for details)].

ray emission from IC scattering of CR electrons in an extended Galactic halo can also produce a very smoothly varying (close to isotropic) spatial distribution that could also be ascribed to the EGB if the size of the halo is large enough (that is, ~ 25 kpc) (Keshet, Waxman & Loeb, 2004). Because the EGB is extracted using gamma-ray data at high Galactic latitudes it is difficult to distinguish between foreground contaminants like an extended halo and the true EGB, so there is no assurance that a detected isotropic component has an extragalactic origin. Nevertheless, we shall continue to use the term EGB when discussing it.

The latest observational contribution to this subject is the *Fermi*-LAT measurement of the spectrum of isotropic diffuse gamma radiation from 200 MeV to 100 GeV (Abdo et al., 2010d). The biggest challenge, and the largest source of systematic uncertainty, in a measurement of the EGB is the subtraction of the various foregrounds. Most important are the diffuse Galactic emission, the contribution from resolved sources, and the instrumental background from misclassified CRs. In the Abdo et al. (2010d) analysis the misidentified CRs were suppressed by applying very stringent event selection criteria, albeit at the expense of efficiency. The diffuse Galactic gamma-ray emission was modeled using the GALPROP code (with particular attention given to characterizing the dominant sources of systematic uncertainties in the foreground modeling; see Section 3.2). The isotropic background was then found using a simultaneous fit of the diffuse Galactic gamma-ray emission from the modeling, resolved sources from the internal *Fermi*-LAT 9-month source list (using the individual localizations but leaving the fluxes in each energy bin to be separately fitted for each source), and a model for the solar IC gamma-ray emission. The fitted isotropic component contained the contributions by misidentified CRs that still passed the event selection and the EGB. The residual particle backgrounds were isotropic over the data taking period for the Abdo et al. (2010d) analysis, estimated using the instrument simulation, and then subtracted from the fitted isotropic component to obtain the EGB. The derived EGB spectrum is shown in Figure 4a. It is a featureless power law, significantly softer than the one obtained from EGRET observations (Sreekumar et al., 1998), as can be seen in Figure 4b. Also, the spectrum does not show a feature at $\gtrsim 2$ GeV found in a reanalysis of the EGRET data with an updated diffuse gamma-ray emission model based on GALPROP (Strong, Moskalenko & Reimer, 2004a).

Using the *Fermi*-LAT-derived EGB, Abdo et al. (2010f) set upper limits on the gamma-ray flux from cosmological annihilation of DM. Figure 4b shows the gamma-ray spectra for representative particle physics models used in the analysis. Several models of varying degree of optimism were considered for the cosmological evolution of structure. WIMP annihilation is very sensitive to the amount of substructure clumping, which enhances the density-squared in the integrand of $J(\psi)$ (Equation 5). The most conservative structure evolution model assumed only the results of a large numerical many-body calculation, and the results for this model are shown in Figure 4b for three representative annihilation final states ($\mu^+\mu^-$, $b\bar{b}$, and $\gamma\gamma$). The more optimistic models treated the substructure contributions by analytically extrapolating to much smaller scales. Different models

for the extragalactic background light were also considered to gauge the effect of gamma-gamma absorption. The most conservative limits for the DM annihilation cross section were obtained assuming that all of the observed emission was due to DM. The limits for the DM annihilation cross sections and masses were: $1.2 \times 10^{-23} \text{ cm}^3 \text{ s}^{-1}$ (for a 1.2 TeV WIMP annihilating to $\mu^+ \mu^-$), $\langle \sigma v \rangle = 5 \times 10^{-25} \text{ cm}^3 \text{ s}^{-1}$ (for a 200 GeV WIMP annihilating to $b\bar{b}$), and $2.5 \times 10^{-26} \text{ cm}^3 \text{ s}^{-1}$ (for a 180 GeV WIMP annihilating to $\gamma\gamma$). Less conservative constraints were derived by first subtracting simple models for the contributions from unresolved star-forming galaxies and blazars [which were modeled assuming power-law spectra with indices -2.7 (star-forming galaxies, motivated by theoretical calculations) and -2.4 (blazars, from observations)]. [Note, the contributions by the different astrophysical source classes to the EGB is not well known. Recent work by the *Fermi*-LAT collaboration (Abdo et al., 2010h) has derived a fraction $< 40\%$ for the contribution by blazars to the EGB. The contributions by other source classes are so far undetermined.] Under these assumptions, very good constraints for the DM annihilation cross section were obtained in the most optimistic scenarios, even excluding the expected thermal WIMP cross section (Equation 2) up to 1 TeV. However, the true upper limits that are based on the conservative assumptions were a factor $10 - 1000$ times higher and realistically do not exclude any of the MSSM parameter space for the annihilation process and cross section.

3.4 Gamma-Ray Line Searches

The cleanest and most convincing DM signal that could be measured would be a monochromatic gamma-ray line on top of the continuum background spectrum. A gamma-ray line would result from decays or annihilations to two-body final states: $\chi(\chi) \rightarrow \gamma X$, where X can be another photon, a Z boson, a Higgs boson, or a non-SM particle (e.g., Bouquet, Salati & Silk, 1989). However, DM models predict branching fractions into such states that are typically $\sim 10^{-4} - 10^{-1}$ compared to the total annihilation or decay rate, placing them below the flux sensitivity of any existing instrument. A search for gamma-ray lines in the range of $0.1 - 10$ GeV was done using EGRET in a $10^\circ \times 10^\circ$ region about the GC with a null result (Pullen, Chary & Kamionkowski, 2007). Most recently, the *Fermi*-LAT team used the first year of survey data to search for gamma-ray lines in the energy range of $30 - 200$ GeV (Abdo et al., 2010c). The analysis used data from two regions: all the sky but the Galactic plane (that is, $|b| \geq 10^\circ$ to avoid the strong diffuse emission from CRs interacting with interstellar gas) and also a $20^\circ \times 20^\circ$ region centered on the GC. Even though source and diffuse emissions are the strongest and most complex around the GC, this region was included in the analysis because the DM concentration also peaks in there, significantly increasing the potential signal. Known point sources were removed by cutting out a 0.2° circular region around each, except within 1° of the GC, in order not to remove this entire region. The resulting spectrum showed no evidence of a line. Flux limits were set at 10 GeV intervals, starting at 30 GeV. For each energy the spectrum was fit to a line shape corresponding to the predicted instrument response and centered on that energy, together with a polynomial background.

For each of three assumed Galactic distributions of DM, the flux limits were translated into cross sections for annihilation to $\gamma\gamma$ or γZ_0 as well as lifetimes for decay to the same final states. See table 1 of Abdo et al. (2010c). The annihilation cross section upper limits were of order $\langle\sigma_{\gamma\gamma}v\rangle \sim 10^{-27} \text{ cm}^3 \text{ s}^{-1}$, and the lifetime lower limits were of order $\tau_{\gamma\gamma} \sim 10^{29} \text{ s}$. Unfortunately, these limits do not significantly constrain the parameter space of DM models for a typical thermal WIMP because of the small branching fractions typically expected for these annihilation or decay modes (an increase in sensitivity of $\sim 100 - 1000$ over the current measurements would be required to constrain canonical thermal WIMP models). Nevertheless, they do disfavor or rule out particular models, such as some that have been constructed to explain the PAMELA rising positron abundance, some that rely on non-thermal production of WIMPs (Equation 2), and models with a thermal cross section but constructed to have a large branching fraction to a gamma-ray line (e.g., Goodman et al., 2011).

3.5 Gamma Rays from Dwarf Spheroidal Galaxies and Satellites

In the standard cosmological model the formation of structure, and of galaxies in particular, is dominated by cold DM (CDM) and proceeds hierarchically, with small structures merging over time into ever larger galaxies and clusters (Blumenthal et al., 1984). Numerical studies of this process predict that the Milky Way should be surrounded by a swarm of smaller structures, including gravitationally unbound streams as well as bound subhalos (Zemp, 2009), many of which would be expected to contain baryonic matter in the form of stars. A couple of dozen Milky Way satellite galaxies are known (Bullock, Kaplinghat & Strigari, 2010), half of them discovered since 2004 by the Sloan Digital Sky Survey (SDSS; York et al., 2000). But that number is small compared to the hundreds predicted by simulations (Klypin et al., 1999; Tollerud et al., 2008). The difference is partly due to the fact that the SDSS has surveyed only $\sim 20\%$ of the full sky, and even in the surveyed regions dim satellites are difficult to detect against the Galactic foreground. Also, SDSS is biased toward seeing the nearer satellites, and those are the most likely to be tidally disrupted. The remaining difference might be understood in terms of truly dark satellites, that is, those without sufficient baryonic matter to form stars. This is supported by studies showing that even many of the known satellites have very low stellar contents compared to their DM masses, the more so for the smaller objects (Simon and Geha, 2007). Several physical processes could prevent baryons from accumulating in small, shallow potential wells, such as heating from early reionization of the universe (Somerville, 2002). Therefore, ongoing searches for DM consider both the known satellites and unknown dark satellites. The former clearly are easier to treat, because their locations are known, as are their approximate mass-to-light ratios.

Dwarf spheroidal (dSph) galaxies (a subclass of the dwarf elliptical galaxies) are the most attractive candidate subhalo objects for DM searches, because these low-luminosity structures are typically found by line-of-sight stellar velocity dispersion measurements to have very high mass-to-light ratios (Bullock, Kaplinghat & Strigari, 2010) and thus abundant DM. They probably also have low astro-

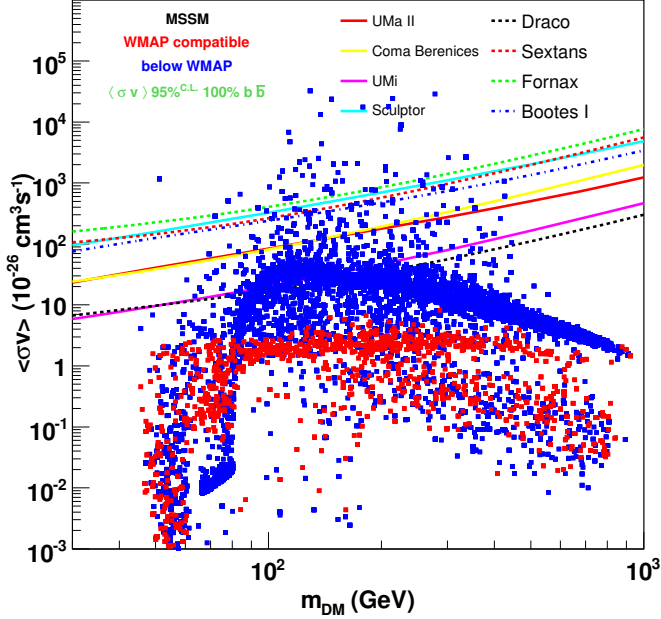


Figure 5 *Fermi*-LAT 95% upper limits for WIMP annihilation to $b\bar{b}$ in selected dSph galaxies in the $(m_{\text{wimp}}, <\sigma v>)$ plane, from Abdo et al. (2010b). The points are derived from a scan over 7 parameters of the Minimal Supersymmetric Standard Model. The red points are the most interesting, as they correspond to a thermal relic density compatible with WMAP data. Thus they roughly correspond to a WIMP annihilation cross section as given by Equation 2, but complex interactions involving multiple supersymmetric partners in the early Universe can change the prediction significantly, as indicated. The blue points represent higher cross sections, and correspondingly lower thermal relic densities, but assume that additional non-thermal production mechanisms contribute to WIMP production, such that WIMPs still comprise all of the dark matter.

physical gamma-ray backgrounds, because they contain almost no gas or dust, no star-forming regions, and probably few millisecond pulsars, compared with globular clusters, which are rich in millisecond pulsars. Because dSphs are small and localized, IACT experiments, as well as the *Fermi*-LAT, can contribute to the search for gamma rays produced by DM annihilation or decay.

The stellar measurements indicate that the known dSphs all have roughly the same mass within their central 300 pc, independent of their luminosities (Strigari et al., 2008), in which case the best targets for indirect detection of DM should be those that are closest to Earth but not obscured by the Galactic disk. Thus far, no statistically significant gamma-ray excess has been detected from any dSph location by any of the gamma-ray telescopes. The *Fermi*-LAT collaboration has published flux upper limits for 14 dSphs based on the first 11 months of data (Abdo et al., 2010b). The limits are presented for several assumptions on the source spectra: power laws of five spectral indices, Γ , ranging from 1 to 2.4 versus DM annihilation for WIMP masses between 10 GeV and 1 TeV. Several

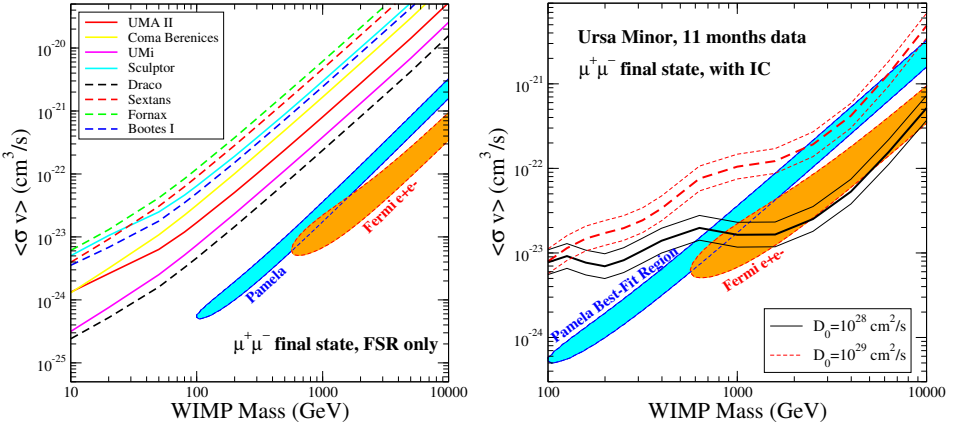


Figure 6 *Fermi*-LAT upper limits for dark matter annihilation to $\mu^+\mu^-$ in dSphs (Abdo et al., 2010b), compared to models that fit well either the PAMELA measurement of the positron fraction or the *Fermi*-LAT measured total electron spectrum. The left panel shows the constraints considering gamma-ray emission from final state radiation only. The right panel shows the constraints for the Ursa Minor dwarf including both final state radiation and emission from inverse Compton scattering of the CMB by the positron and electron muon-decay products, for two different assumptions for the cosmic ray diffusion coefficient. The bands indicate the effect of uncertainties in the Ursa Minor dark matter density profile. Including the inverse Compton contribution improves the upper limit, but at the expense of using a model dependent upon an unconstrained diffusion coefficient.

final states are considered for the DM annihilation, including $b\bar{b}$, W^+W^- , $\tau^+\tau^-$, and $\mu^+\mu^-$. For $\Gamma = 2$ the typical integral flux upper limit above 100 MeV for a single dSph location is a few times 10^{-9} photons $\text{cm}^{-2} \text{s}^{-1}$.

To interpret the flux limits as constraints on DM annihilation or decay requires knowledge of the amount of DM in each dSph. In addition, DM annihilation is highly sensitive to the radial distribution and central concentration of the WIMPs, as it is proportional to the square of the density (Equation 4). The stellar line-of-sight velocity dispersion measurements are effective in constraining the dSph mass and, to some degree, the DM distribution within; but they cannot measure the shape of the central DM cusp, let alone small-scale clumping, to a degree that would allow a completely model-independent assessment of the geometrical part of Equation 4. Therefore, the *Fermi*-LAT analysis assumes a smooth Navarro-Frenk-White profile (Navarro, Frenk & White, 1997) out to the dSph tidal radius r_t (see Read et al. (2005)), conservatively with no boost from substructure or possible long-range attractive interactions between WIMPs (Sommerfeld enhancement, e.g., Arkani-Hamed et al., 2009). For each dSph, the Navarro-Frenk-White characteristic density ρ_s and scale radius r_s must be evaluated from the stellar data via an involved procedure (Abdo et al., 2010b) that relies on prior probabilities for r_s and ρ_s derived from Λ CDM simulations (Diemand, Kuhlen & Madau, 2007; Springel et al., 2008) as well as prior probabilities

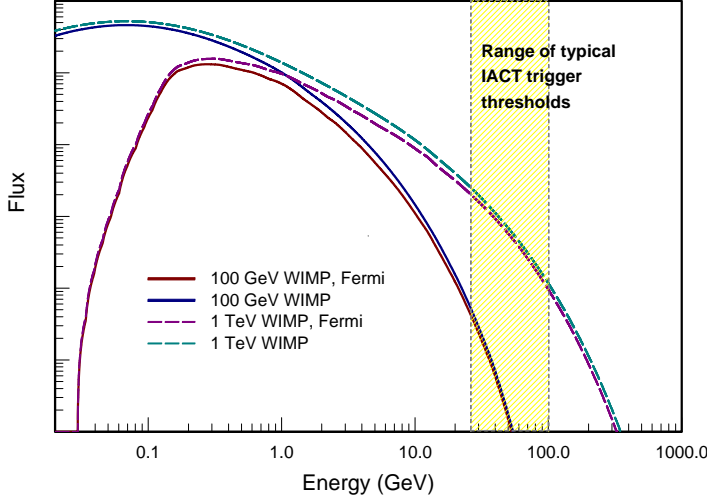


Figure 7 The spectrum of detected gamma rays from dark matter annihilation to $b\bar{b}$, as predicted by DarkSUSY for WIMPs of 100 GeV and 1 TeV mass. In each case the rate is compared between an ideal 1 m^2 instrument and the *Fermi*-LAT, taking into account its effective area vs. energy for “diffuse-class” events (Atwood et al., 2009). The range of *trigger* thresholds for ground-based Imaging Air Cherenkov Telescopes is also shown, indicating that their sensitivity to this final state, even with their $> 10,000 \text{ m}^2$ effective areas (but higher background and shorter observing time), is relatively small until the WIMP mass exceeds a TeV.

for the stellar mass-to-light ratio and the velocity dispersion anisotropy. In the case that photons come from DM decay rather than annihilation, the astrophysical model is less critical, as the flux is then simply proportional to the amount of DM mass along the line of sight and within the instrument PSF. However, Abdo et al. (2010b) do not provide limits for decay lifetimes.

In Abdo et al. (2010b) only a select 8 of the 14 dSphs are used to set limits for the DM annihilation cross section. Results are shown versus WIMP mass for each of the 8 in Figure 5, where each red or blue point represents the theoretical prediction of the MSSM for a given set of model parameters. The red points have a thermal relic abundance corresponding to the inferred cosmological DM density, thus forming a band along the standard cross section of Equation 2, where the deviations from that standard follow from model details such as the spectrum of supersymmetric partners that “co-annihilate” in the early Universe. That is, before freeze-out in the early Universe there may have been multiple supersymmetric particle types of similar mass interacting, not just the lightest supersymmetric partner that is the DM WIMP, so the relic abundance depends

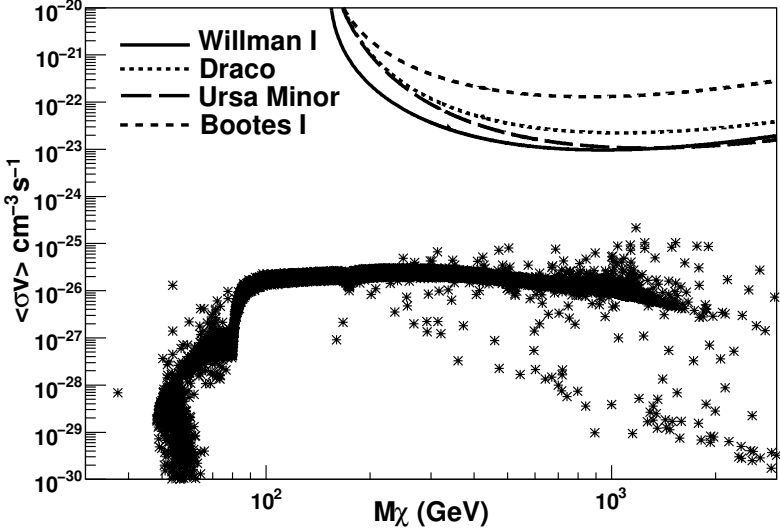


Figure 8 DM annihilation upper limits from observations of four dSphs by VERITAS, from Acciari et al. (2010). The $\Phi_s(E)$ from Equation 3 is taken to be a sum over final states with branching fractions from a generic model, but it is comparable to assuming a 100% $b\bar{b}$ final state. Black asterisks represent minimal supersymmetric model predictions for neutralino WIMPs with thermal relic abundance corresponding to the inferred cosmological dark matter density.

on more than just the annihilation cross section of the WIMP. The blue points represent models with higher annihilation cross sections, corresponding to lower thermal relic densities. They still assume that WIMPs comprise all of the dark matter and thus rely on esoteric models in which there are additional non-thermal production processes. Similar plots are provided by Abdo et al. (2010b) for other particle physics models, including Kaluza-Klein universal extra dimensions and mSUGRA, but the main point here is that with $\sim 10 - 20\%$ of the eventual complete *Fermi*-LAT data set in hand, the limits from individual dSphs are still a factor of 10 or more above the most interesting parameter space pointed to by Equation 2.

The dSph Segue 1 is not included in the analysis by Abdo et al. (2010b) because of controversy over whether it is a dSph or merely a star cluster stripped from the Sagittarius galaxy (Niederste-Ostholt et al., 2009). A more recent publication makes a strong case, based on recent spectroscopic observations, for it to be a dSph and, in fact, the most DM-dominated galaxy known (Simon et al., 2010). It is arguably the best target for DM searches, due to its proximity (only 25 kpc from the Sun) and high Galactic latitude, as well as its high DM mass. The *Fermi*-LAT collaboration has not yet presented DM limits from Segue 1, but analyses based on flux limits from 9 months of data have been published by subsets of collaboration members (Scott et al., 2009; Essig et al., 2010). Besides including more dwarfs such as Segue 1, the results of Abdo et al. (2010b) will be

strengthened by an ongoing combined analysis of all dSphs.

For $\mu^+\mu^-$ final states the only direct gamma-ray signal comes from the hard E^{-1} photon spectrum of final-state radiation ($\tau^+\tau^-$ final states are similar but do also produce some photons from π^0 decay). However, additional lower-energy photons are generated by IC scattering of the CMB (which is the dominant radiation field in dSphs due to the paucity of stars and dust) by high-energy electrons and positrons from μ^\pm decay as they propagate through the galaxy. The IACTs, with their high energy thresholds, would not see that secondary production, but for the *Fermi*-LAT it can comprise a significant fraction of the signal. This complicates the analysis by introducing a dependence on CR propagation in the dSph, which is not necessarily well described by the same models used to describe CR propagation in the Milky Way. Nevertheless, the analysis employs the usual diffusion-loss equation, solved in spherical symmetry with free-escape boundary conditions. The results depend on the diffusion coefficient, which is not constrained by any existing data but can only be assumed to be in the neighborhood of the value relevant to the Milky Way. A larger coefficient results in more of the photon signal being produced outside of the vicinity of the dSph covered by the telescope PSF, and therefore less signal significance. Figure 6 shows the *Fermi*-LAT limits for the DM annihilation cross section for the case of a $\mu^+\mu^-$ final state (Abdo et al., 2010b). Figure 6a assumes photon production only by final-state radiation, whereas the Figure 6b shows the effect, for a single dSph, of including IC scattering. In the latter interpretation, data from just a single dSph have excluded much of the parameter space of DM models devised to explain the PAMELA and *Fermi*-LAT positron and electron results described in Section 3.1.

IACTs can produce competitive limits for DM annihilation in dSphs only for very high WIMP masses or with leptonic or $\gamma\gamma$ final states because of their relatively high energy thresholds. As illustrated in Figure 7, even for annihilation of 1 TeV WIMPs into $b\bar{b}$, almost all of the photons are well below the IACT thresholds. Of the existing IACTs, MAGIC has the lowest threshold and, therefore, should achieve the best sensitivity to DM. The MAGIC collaboration has published flux upper limits above 100 GeV for the dSphs Draco and Willman 1 from observations made by the first of the two 17-m MAGIC telescopes (Lombardi et al., 2009). Comparing with predictions from four representative mSUGRA models, the MAGIC collaboration finds the expected fluxes to be at least three orders of magnitude below their upper limits. [Note some caution should be used when considering the limits derived for Willman 1, because Willman et al. (arXiv:1007.3499) state that foreground contamination in their observations and the unusual stellar kinematic distribution mean that the DM mass for Willman 1 is not robustly determined. Consequently, the constraints from X-rays and gamma rays that assume an equilibrium DM model are strongly affected by the systematic uncertainties in their optical observations.]

The HESS experiment has published DM limits from observations made on four dwarf galaxies: Sagittarius, Carina, Sculptor, and Canis Major, of which the first is classified as a dwarf elliptical and the last as a dwarf irregular (Aharonian et al., 2008a, 2009a; Glicenstein, 2010). The upper limits for cross section, assuming

annihilation into gauge-boson-pair (W, Z) final states, have minima for WIMP masses $M_\chi \sim 1 - 2$ TeV. Glicenstein (2010) compares the HESS Sculptor limits to the corresponding limits from the *Fermi*-LAT (a $b\bar{b}$ final state was assumed in the latter case, but that does not make a very large difference in the photon spectrum). The HESS cross section minimum near 2 TeV is nearly equal to an extrapolation of the *Fermi*-LAT limit, but below that WIMP mass it is not competitive.

VERITAS has observed four dSphs with energy thresholds ranging from 300 GeV to 380 GeV: Draco, Ursa Minor, Bootes 1, and Willman 1 (Acciari et al., 2010), of which only the last was not included in the *Fermi*-LAT DM limits. The upper limits show a broad minimum around 1 TeV, with the best cases, Willman 1 and Ursa Minor, at $\langle\sigma v\rangle \approx 10^{-23} \text{ cm}^3 \text{ s}^{-1}$ (see Figure 8). This is a factor of a few higher than the corresponding *Fermi*-LAT upper limit from Ursa Minor, although an exact comparison is difficult owing to different assumptions about the composition of the final state as well as the astrophysical factors. In general, none of the gamma-ray observations from dSph locations come close to the most interesting model space except for the *Fermi*-LAT results for WIMP masses < 100 GeV.

So far, no DM limits have been derived from neutrino observations of dwarf galaxies. The relevance of neutrino observations is thoroughly explored by Sandick et al. (2009) within the context of leptonic models such as those developed to explain the PAMELA positron excess. In short, the IceCube experiment will contribute at the very high-mass end, for example, in the case of WIMPs of mass greater than 7 TeV annihilating to muon pairs. Of course, it would be the only suitable type of experiment if the WIMPs were to annihilate or decay primarily to neutrinos!

Detecting DM annihilation or decay in satellite galaxies that are truly dark or have not yet been detected in the optical is more difficult, both in execution and interpretation. Thus far, no DM cross section or lifetime limits have been placed by collaboration analyses of unidentified sources in *Fermi*-LAT data, although preliminary reports of a null result from 10 months of observation have been given based on work in progress (Wang, 2009; Bloom, 2010). The difficulty with interpretation is that to predict how many dark satellites should be detected for a given annihilation cross section and WIMP mass, for example, requires a very detailed model of the Galactic DM distribution. Models based on many-body simulations, such as Via Lactea-II (Diemand et al., 2008), Aquarius (Springel et al., 2008), or GHALO (Zemp, 2009), are candidates, but multiple realizations of a given model are needed in order to account statistically for the unknown position of the Solar System with respect to the DM subhalos.

For this topic, the searching has to be done by an all-sky instrument such as the *Fermi*-LAT, but the IACTs could play an important role in terms of follow-up observations of candidates. Data analyses start from the list of unidentified sources in the the first *Fermi*-LAT catalog (1FGL), which was derived for the first 11-months of LAT data (Abdo et al., 2010g). In the work presented by Bloom (2010), sources are selected to eliminate those in the Galactic plane ($|b| \leq 10^\circ$)

or those that exhibit transient behavior. Then two test statistics are evaluated: one to test whether the source spectrum is more consistent with DM ($b\bar{b}$ or $\mu^+\mu^-$ final states) than with a simple power law, and another to test whether the source is significantly extended versus being consistent with a point source. Candidates passing cuts on the test statistics are carefully studied to avoid backgrounds such as two overlapping point sources. Background sources can be further reduced by multiwavelength studies of the candidate locations (Baltz et al, 2006). By this procedure, the analysis reported by Bloom (2010) found no dark satellite candidates in the first 10 months of *Fermi*-LAT data, but no upper limits were given. However, estimates of the *Fermi*-LAT sensitivity to dark satellites have been published elsewhere. Baltz et al. (2008) showed that, for 100 GeV WIMPs annihilating with the cross section of Equation 2 and a semianalytic model of the DM distribution, a dozen satellites are expected to be detected at 5σ significance or better in a five-year mission. Another recent study, based on the Via Lactea-II many-body simulation, is less optimistic, predicting for the same WIMPs between one and five detections at 3σ significance in a 10-year mission (Anderson et al., 2010). However, the same work also predicts that for nearly all of the dark satellites detected with $> 3\sigma$ significance a non-point-like extension is expected to be seen at $\gtrsim 5\sigma$ significance, which is encouraging for analyses that rely heavily on the source extension to eliminate background.

Analyses that consider only the spectra of unidentified sources can be interesting, however, not only for small or distant subhalos that cannot be resolved but also for postulated point-like DM sources, such as DM concentrations around intermediate mass black holes (Bertone, Zentner & Silk, 2008). Baltz et al. (2008) explored the sensitivity of the *Fermi*-LAT to such sources prior to launch, but that was primarily a consideration of the point-source sensitivity of the instrument, a topic by now very well studied during the preparation of the 1FGL (Abdo et al., 2010g). The remaining difficulty is distinguishing such sources from background via spectral analysis. Detecting a large population of candidates all fitting a single, large WIMP mass would be the ideal signal, but that has not happened. Recently, Sandick et al. (2010) explored this subject without doing detailed spectral analysis. They concluded that many (or even all!) of the 368 *Fermi*-LAT unidentified sources at least 10° from the Galactic plane and of at least 5σ significance could be due to DM. However, rather than try to put a constraint on DM, they turned the argument around and attempted to constrain the astrophysics and cosmology.

3.6 Galaxy Clusters

Galaxy clusters are the most massive collapsed structures in the Universe and are known to be DM dominated. X-ray studies of the hot intergalactic gas show that not only is there more mass in the gas than in the galaxies themselves, typically by a factor of two, but for the gas to be in hydrostatic equilibrium there must be several times more mass in DM than in the gas or galaxies (e.g., Reiprich & Boehringer, 2002; Vikhlinin et al., 2006). Clusters are more distant than local dwarfs, but they are also far more massive and are therefore attractive targets for

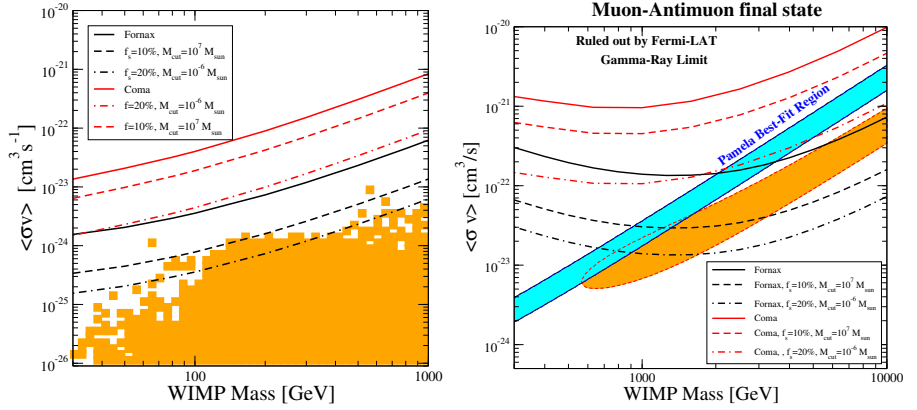


Figure 9 *Fermi*-LAT upper limits from Ackermann et al. (2010b) for the dark matter annihilation cross-section for a $b\bar{b}$ final state (left panel) and a $\mu^+\mu^-$ final state (right panel) for the Coma and Fornax clusters, including the effect of substructure on the expected gamma-ray signal. The constraints are shown for no substructure (solid lines), substructure down to the scale of dwarf galaxies (dashed lines), and substructure down to $10^{-6} M_\odot$ (dot-dashed lines). The orange points in the left panel shows the predicted cross section for a set of minimal supersymmetric models that have thermal relic densities compatible with the observed universal dark matter density, similar to the red points in Figure 5. The contours in the right panel show regions allowed by dark matter models that provide good fits to the PAMELA positron fraction (blue) or the *Fermi*-LAT total electron spectrum (orange).

DM searches. However, they also sometimes contain intense gamma-ray sources in the form of AGN. The typical angular size of even nearby clusters (a few tenths of a degree to a degree) is comparable or smaller than the *Fermi*-LAT PSF except at GeV or greater energies, so it is difficult or impossible to subtract the contribution of a single AGN (for IACTs the PSF is $\sim 0.1^\circ$, comparable to that of the thin section of the *Fermi*-LAT $\gtrsim 10$ GeV). Apart from those containing known AGN or radio galaxies (such as M87 in the Virgo cluster or NGC 1275 in Perseus), no gamma-ray signal has yet been associated with a galaxy cluster. The best flux upper limits below 100 GeV come from the *Fermi*-LAT, for 33 clusters (Ackermann et al., 2010a) observed over 11 months, typically at the level of a few times $10^{-9} \text{ cm}^2 \text{ s}^{-1}$. The IACTs CANGAROO, HESS, MAGIC, and VERITAS between them have reported upper limits from observations of six galaxy clusters (Kiuchi, 2009; Aharonian et al., 2009b,c; Aleksic et al., 2010; Perkins, 2009), three of which are not included in the *Fermi*-LAT publication. The flux limits obtained by the IACTs for high-mass WIMPs are three to four orders of magnitude below those of the *Fermi*-LAT, reflecting the very large effective areas of the IACTs (albeit with much shorter observation times). However, the *Fermi*-LAT sensitivity is better for many sources because of the much higher energy thresholds of the IACTs. For example, in the Perseus cluster the radio galaxy NGC 1275 is strongly detected by the *Fermi*-LAT (Abdo et al., 2009c), but only

upper limits have followed from IACT observations (Aleksic et al., 2010; Acciari, 2009).

Translating the flux limits to DM limits is more model dependent than for dSphs observations. Clusters are expected to include CR proton and electron populations that would produce gamma rays through collisions with the intergalactic medium and through IC scattering on the CMB and intracluster radiation field (Jeltema, Kehayias & Profumo, 2009). This significantly complicates the interpretation of a signal but may be ignored when setting conservative DM limits. However, the DM spatial distribution is critical to limits for DM annihilation because the rate is proportional to density squared. X-ray studies provide a scale radius and DM total mass for each cluster. Unlike the case of dSphs, for which boosts from substructure are not expected to be important (and are typically ignored in setting limits, to be conservative), substructure is likely to be important in clusters from the galactic scale on down. At the very least, clusters obviously are full of structure on the galaxy and dwarf-galaxy scales, so ignoring substructure entirely would run the risk of setting an overly conservative limit.

The *Fermi*-LAT collaboration has published DM limits from observations of six galaxy clusters (Ackermann et al., 2010b). Navarro-Frenk-White profiles are assumed for the DM distributions, with the scale densities and radii calculated from the cluster virial masses, as determined from X-ray observations (Reiprich & Boehringer, 2002) together with the the X-ray concentration-virial mass relation from Buote et al. (2007). Any DM signal from clusters is assumed to be unresolvable by the *Fermi*-LAT, as the Navarro-Frenk-White scale radii lie between only 0.26° and 0.45° , and the signal would be further concentrated by the density-squared dependence of the annihilation rate. Both $b\bar{b}$ and $\mu^+\mu^-$ final states are considered. In the latter case, IC scattering of final-state electrons from the CMB is included and, in fact, dominates within the *Fermi*-LAT acceptance for WIMP masses above a few hundred GeV.

With no substructure assumed, the resulting conservative limits are not as good as those in Abdo et al. (2010b) for dSphs. At 100 GeV they are at best a factor of ~ 100 above Equation 2. Figure 9 shows the annihilation cross section upper limits from the *Fermi*-LAT for two of the six clusters, the best and worst cases, including the improvements that result from assuming substructure. For the best case, which is the Fornax cluster with substructure down to $10^{-6}M_\odot$, the upper limits are nearly equal to those obtained from the best-case *Fermi*-LAT dSph observation for $b\bar{b}$ final states. The more conservative assumption of substructure down to the dwarf galaxy level gives upper limits about three times higher in the best case.

Only one of the clusters observed by the IACTs (Coma) is included in the *Fermi*-LAT limits for DM annihilation. As in the case of dSph observations, the high threshold energies of IACTs prevents them from being sensitive to low-mass WIMPs, especially for non-leptonic final states. In fact, the IACT publications do not include DM interpretations at all, except in one case, the MAGIC observation of the Perseus cluster given by Aleksic et al. (2010). A direct comparison to a *Fermi*-LAT result is not possible, but the conclusion of these researchers is that

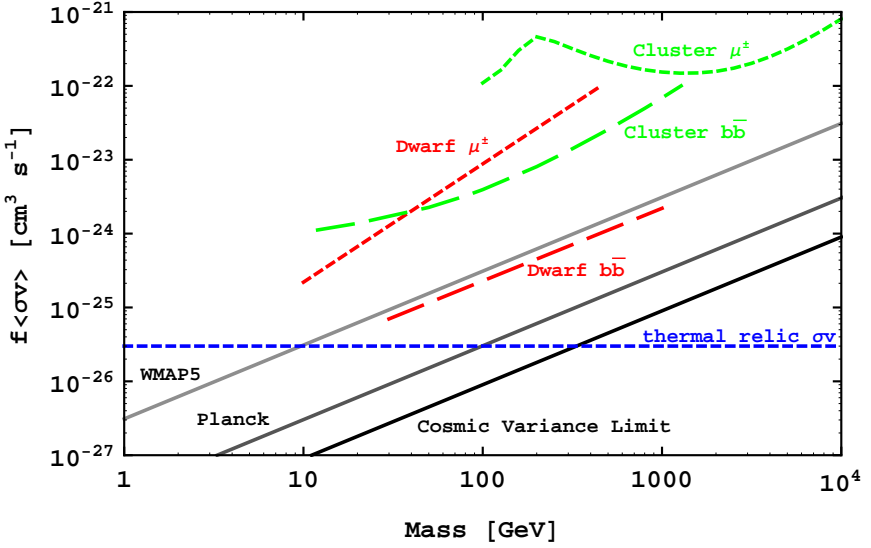


Figure 10 Constraints on the DM annihilation cross section $\langle\sigma v\rangle$ from various instruments. The gamma-ray limits are shown for dwarf spheroid galaxies for μ^\pm (red short-dashed line) and $b\bar{b}$ (red long-dashed line), and galaxy clusters for μ^\pm (green short-dashed line) and $b\bar{b}$ (green long-dashed line) final states, respectively. The CMB-derived limit (for all annihilation channels except neutrinos) using WMAP 5-year data is shown as the light grey line, projected limits for Planck are shown as the medium grey line, and the dark grey line shows the ultimate cosmic variance limit on the possible reach of this technique (reproduced from Galli et al., 2009). For the CMB limits, f parameterizes the coupling of the annihilation products to the gas in the early Universe and is usually $\mathcal{O}(1)$. The dashed blue line shows the thermal self-annihilation cross section given by Equation 2.

a boost (from substructure and/or Sommerfeld enhancement) of at least 10^4 is needed in order to be sensitive to a MSSM model with the highest f_{SUSY} factor, as defined by Sánchez-Conde et al. (2007).

4 OUTLOOK

As of the date of this review, there has been no definitive detection of a DM signal in astroparticle data. This does not mean that no CRs or gamma rays from DM have been detected. Rather, given the astrophysical uncertainties associated with interpreting the data, where a signal has been detected, there is insufficient evidence to allow unambiguous attribution to DM annihilation or decay scenarios. Thus far, the astroparticle data have been most useful for limiting the properties of proposed DM particles in the contexts of specific models. In this review, we discussed the most recent experimental results together with the related astrophysical phenomenology to provide an understanding of issues associated with interpreting the data. Understanding these uncertainties and how they can be quantified and/or reduced is essential to further progress in this area of research.

The PAMELA rising positron abundance remains intriguing, but its interpretation is ambiguous. DM explanations for these data, whether invoking WIMP decay or annihilation, have not been completely ruled out by recent gamma-ray data. However, given the non-standard nature of these DM models and the existence of reasonable alternative astrophysical explanations, the DM explanation is inconclusive.

AMS-02 (Bindi, 2010) is expected to launch in early 2011. It will significantly improve on current CR observations, especially for positrons and antiprotons. For example, the enhanced particle-identification capabilities of AMS-02 will clarify whether the PAMELA positron measurements are contaminated by misidentified protons, and they will extend the positron data to higher energies. This is likely to improve the indirect search for DM in general (Beischer et al., 2009) and the interpretation of the PAMELA positron abundance in particular.

Future results from gamma-ray telescopes, the *Fermi*-LAT in particular, will show significantly improved sensitivity to DM annihilation or decay. Searches for DM in the halo of the Milky Way with the *Fermi*-LAT data are underway. DM halo searches have the advantage of large numbers of signal photons, but their potential will only be realized, in terms of approaching sensitivity to the most interesting models, if better constraints can be put on the large Galactic diffuse background. That will require better understanding of the propagation of CRs in the Galaxy as well as improved knowledge of the gas distributions and ISRF. It has long been expected that a DM signal may be detectable toward the GC because the annihilation rate should peak in this region. But, the numerous point sources, together with the inter-relationship with the diffuse emission and its uncertainties along the line-of-sight, and instrumental effects make analysis complicated. As for the halo searches, improvements in understanding the foreground emission, together with source identification, are crucial for this kind of analysis. However, the DM limits from observations of dwarf spheroidal satellite galaxies are sure to improve steadily as the *Fermi*-LAT accumulates up to 10 times more data than have been used to set limits so far. The statistical power will further improve as more sophisticated analyses make simultaneous fits to the ensemble of dwarfs and as more dwarfs are discovered by upcoming optical surveys that will greatly improve the sky coverage (e.g. DES (Abbott et al., 2006), BigBOSS (Schlegel et al., 2009), Pan-STARRS, LSST (Abel et al., 2009)). Further stellar-velocity observations of dwarfs are also likely to improve knowledge of the astrophysical factors (Equation 4). Therefore, it is reasonable to expect that by the end of the *Fermi*-LAT mission the dwarf analyses will be sensitive to annihilation of WIMPs into heavy quarks or gauge bosons at or below the standard annihilation cross section, Equation 2, for WIMP masses up to at least $100 \text{ GeV } c^{-2}$.

Of course, within the time frame of the *Fermi*-LAT mission, the Large Hadron Collider experiments will explore the parameter space in certain particle physics models for production of WIMPs up to much higher masses than $100 \text{ GeV } c^{-2}$ (Hooper & Baltz, 2008). If such a particle is discovered, then the indirect detection experiments will not only be important for studying its possible role as

a DM particle, but they may also have much more information to work with, in particular the WIMP mass and strengths of couplings to the standard model.

In the near term, the CMB also provides a method for detecting or constraining particle DM that is potentially competitive with the astroparticle searches. Because the number of DM particles remains constant after freeze-out, their number density varies as $n \propto z^3$, where z is the redshift. Because the annihilation rate per unit volume is $\sim n^2 \langle \sigma v \rangle$, annihilation is greatly enhanced at early times. In particular, the annihilation rate around the time of recombination, $z \sim 1000$, could have been large enough to affect the CMB significantly. If the products of DM annihilation were anything besides neutrinos, they would have coupled to the surrounding gas and caused significant reionization. This leads to a relatively strong constraint from current WMAP data, which exclude DM with the standard annihilation cross section (Equation 2) and mass $\lesssim 10 \text{ GeV } c^{-2}$. The current limit using this method is shown in Figure 10, which also summarizes the limits derived from gamma-ray data discussed earlier. Future data from the Planck satellite (Tauber, 2010) will cover a larger region of WIMP parameter space, either detecting or excluding DM with the standard annihilation cross section up to $\sim 100 \text{ GeV } c^{-2}$. For a more thorough discussion see Galli et al. (2009, and references therein). Along with gamma-ray observations, measurements of the CMB by instruments like Planck constitute one of the most interesting possibilities for detecting or constraining the properties of DM in the near future.

Acknowledgements

We are grateful for the assistance and comments by the following people: B. Anderson, W. Atwood, S. Digel, T. Jeltema, P. Michelson, I. Moskalenko, S. Murgia, E. Murphy, J. Nielsen, S. Profumo, S. Ritz, and L. Strigari. We acknowledge the assistance of E. Mocchiutti and P. Picozza in the preparation of Figure 1.

References

- Abbasi R, Abdou Y, Ackermann M, Adams J, Ahlers M, *et al.* [IceCube Collab.]. 2009. *Phys. Rev. Lett.* 102:201302
- Abbasi R, Abdou Y, Abu-Zayyad T, Adams J, Aguilar JA, *et al.* [IceCube Collab.]. 2010. *Phys. Rev. D* 81:057101
- Abbott T, Aldering G, Annis J, Barlow M, Bebek C, *et al.* [Dark Energy Survey Collab.]. 2006. 17th *Int. Conf. Part. Nucl., Santa Fe, N.M., AIP Conf. Proc.* 842:989 (astro-ph/0510346)
- Abdo A A, Ackermann M, Atwood W B, Bagaglia R, Baldini L, *et al.* [*Fermi*-LAT Collab.]. 2009a. *Ap. J.* 696:1084
- Abdo A A, Ackermann M, Ajello M, Atwood W B, Axelsson M, *et al.* [*Fermi*-LAT Collab.]. 2009b. *Phys. Rev. Lett.* 102:181101
- Abdo A A, Ackermann M, Ajello M, Asano K, Baldini L, *et al.* [*Fermi*-LAT Collab.]. 2009c. *Ap. J.* 699:31

Abdo A A, Ackermann M, Ajello M, Anderson B, Atwood W B, *et al.* [*Fermi*-LAT Collab.]. 2009d. *Phys. Rev. Lett.* 103:251101

Abdo A A, Ackermann M, Ajello M, Baldini L, Ballet J, *et al.* [*Fermi*-LAT Collab.]. 2010a. *Ap. J.* 710:133

Abdo A A, Ackermann M, Ajello M, Atwood W B, Baldini L, *et al.* [*Fermi*-LAT Collab.]. 2010b. *Ap. J.* 712:147

Abdo A A, Ackermann M, Ajello M, Atwood W B, Baldini L, *et al.* [*Fermi*-LAT Collab.]. 2010c. *Phys. Rev. Lett.* 104:091302

Abdo A A, Ackermann M, Ajello M, Atwood W B, Baldini L, *et al.* [*Fermi*-LAT Collab.]. 2010d. *Phys. Rev. Lett.* 104:101101

Abdo A A, Ackermann M, Ajello M, Allafort A, Atwood W B, *et al.* [*Fermi*-LAT Collab.]. 2010e. *Ap. J.* 713:154

Abdo A A, Ackermann M, Ajello M, Baldini L, Ballet J, *et al.* [*Fermi*-LAT Collab.]. 2010f. *J. Cosmol. Astropart. Phys.* 1004:14

Abdo A A, Ackermann M, Ajello M, Allafort A, Antolini E, *et al.* [*Fermi*-LAT Collab.]. 2010g. *Ap. J. Supp.* 188:405

Abdo A A, Ackermann M, Ajello M, Antolini E, Baldini L, *et al.* [*Fermi*-LAT Collab.]. 2010h. *Ap. J.* 720:435

Abel P A, Allison J, Anderson S F, Andrews J R, Angel R P, *et al.* [LSST Science Collab.s and LSST Project Collab.]. 2009. (arXiv:0912.0201)

Abraham J, Aglietta M, Aguirre I C, Albrow M, Allard D, *et al.* [*Pierre Auger* Collab.]. 2004. *Nucl. Instrum. Methods Phys. Res. A* 523:50

Acciari V A, Aliu E, Arlen T, Aune T, Bautista M, *et al.* [VERITAS Collab.]. 2009. *Ap. J. Lett.* 706:275

Acciari V A, Arlen T, Aune T, Beilicke M, Benbow W, *et al.* [VERITAS Collab.]. 2010. *Ap. J.* 720:1174

Ackermann M, Ajello M, Allafort A, Baldini L, Ballet J, *et al.* [*Fermi*-LAT Collab.]. 2010a. *Ap. J. Lett.* 717:71

Ackermann M, Ajello M, Allafort A, Baldini L, Ballet J, *et al.* [*Fermi*-LAT Collab.]. 2010b. *J. Cosmol. Astropart. Phys.* 1005:025

Ackermann M, Ajello M, Atwood W B, Baldini L, Ballet J, *et al.* [*Fermi*-LAT Collab.]. 2010c. *Phys. Rev. D* 82:092004

Ackermann M, Ajello M, Baldini L, Ballet J, Barbiellini G, *et al.* [*Fermi*-LAT Collab.]. 2010d. *Ap. J.* 726:81

Adriani O, Barbarino G C, Bazilevskaya G A, Bellotti R, Boezio M, *et al.* [PAMELA Collab.]. 2009a. *Nature* 458:607

Adriani O, Barbarino G C, Bazilevskaya G A, Bellotti R, Boezio M, *et al.* [PAMELA Collab.]. 2009b. *Phys. Rev. Lett.* 102:051101

Adriani O, Barbarino G C, Bazilevskaya G A, Bellotti R, Boezio M, *et al.* [PAMELA Collab.]. 2010a. *Astropart. Phys.* 34:1

Adriani O, Barbarino G C, Bazilevskaya G A, Bellotti R, Boezio M, *et al.* [PAMELA Collab.]. 2010b. *Phys. Rev. Lett.* 105:121101

Aguilar M, Alcaraz J, Allaby J, Alpat B, Ambrosi G, *et al.* [AMS Collab.]. 2002. *Phys. Rep.* 366:331

Aharonian F A and Atoyan A M. 1991. *J. Phys. G* 17:1769

Aharonian F A, Atoyan A M, and Völk H J. 1995. *Astron. & Astrophys.* 296:L41

Aharonian F, Akhperjanian A G, Bazer-Bachi A R, Beilicke M, Benbow W, *et al.* [HESS Collab.]. 2006. *Ap. J.* 636:777

Aharonian F, Akhperjanian A G, Bazer-Bachi A R, Beilicke M, Benbow W, *et al.* [HESS Collab.]. 2008a. *Astropart. Phys.* 29:55. Erratum. 2008. *Astropart. Phys.* 33:274

Aharonian F, Akhperjanian A G, Barres de Almeida U, Bazer-Bachi A R, Becherini Y, *et al.* [HESS Collab.]. 2008b. *Phys. Rev. Lett.* 101:261104

Aharonian F, Akhperjanian A G, Barres de Almeida U, Bazer-Bachi A R, Behera B, *et al.* [HESS Collab.]. 2009a. *Ap. J.* 691:175

Aharonian F, Akhperjanian A G, Anton G, Barres de Almeida U, Bazer-Bachi A R, *et al.* [HESS Collab.]. 2009b. *Astron. & Astrophys.* 495:27

Aharonian F, Akhperjanian A G, Anton G, Barres de Almeida U, Bazer-Bachi A R, *et al.* [HESS Collab.]. 2009c. *Astron. & Astrophys.* 502:437

Aharonian F, Akhperjanian A G, Anton G, Barres de Almeida U, Bazer-Bachi A R, *et al.* [HESS Collab.]. 2009d. *Astron. & Astrophys.* 508:561

Ahmed Z, Akerib D S, Arrenberg S, Bailey C N, Balakishiyeva D, *et al.* [CDMS-II Collab.]. 2010. *Science* 327:1619

Anchordoqui L A and Montaruli T. 2010 *Annu. Rev. Nucl. Part. Sci.* 60:129

Aleksić J, Antonelli L A, Antoranz P, Backes M, Baixeras C, *et al.* [MAGIC Collab.]. 2010. *Ap. J.* 710:634

Anderson B, Kuhlen M, Diemand J, Johnson R P, Madau P. 2010. *Ap. J.* 718:899

Ando S and Pavlidou V. 2009. *MNRAS* 400:2122

Appelquist T, Cheng H C, and Dobrescu B A. 2001. *Phys. Rev. D* 64:035002

Aprile E, Arisaka K, Arneodo F, Askin A, Baudis L, *et al.* [XENON100 Collab.]. 2010. *Phys. Rev. Lett.* 105:131302

Arkani-Hamed N, Finkbeiner D P, Slatyer T R, and Weiner N. 2009. *Phys. Rev. D* 79:015014

Arvanitaki A, Dimopoulos S, Dubovsky S, Graham P W, Harnik R, and Rajendran S. 2009. *Phys. Rev. D* 79:105022

Asaoka Y, Shikaze Y, Abe K, Anraku K, Fujikawa M, *et al.* 2002. *Phys. Rev. Lett.* 88:051101

Asztalos S J, Rosenberg L J, van Bibber K, Sikivie P, and Zioutas K. 2006. *Annu. Rev. Nucl. Part. Sci.* 56:293

Asztalos S J, Carosi G, Hagmann C, Kinion D, van Bibber K, *et al.* [ADMX Collab.]. 2010. *Phys. Rev. Lett.* 104:041301

Atkins R, Benbow W, Berley D, Blaufuss E, Bussons J, *et al.* [MILAGRO Collab.]. 2003. *Ap. J.* 595:803

Atoyan A M, Aharonian F A, and Völk H J. 1995. *Phys. Rev. D* 52:3265

Atwood W B, Bagagli R, Baldini L, Bellazzini R, Barbiellini G, *et al.* 2007. *Astropart. Phys.* 28:422

Atwood W B, Abdo A A, Ackermann M, Althouse W, Anderson B, *et al.* [Fermi-LAT Collab.]. 2009. *Ap. J.* 697:1071

Babson J, Barish B, Becker-Szendy R, Bradner H, Cady R, *et al.* 1990. *Phys. Rev. D* 42:3613

Balkanov V, Belolaptikov I, Bezrukov L, Budnev N, Capone A, *et al.* [Baikal Collab.]. 2003. *Nucl. Instrum. Methods Phys. Res. A* 498:231

Baltz E A, Battaglia M, Peskin M E, and Wizansky T. 2006. *Phys. Rev. D* 74:103521

Baltz E A, Taylor J E, and Wai L L. 2007. *Ap. J. Lett.* 659:125

Baltz E A, Berenji B, Bertone G, Bergström L, Bloom E, *et al.* 2008. *J. Cosmol. Astropart. Phys.* 0807:013

Barbiellini G, Basini G, Bellotti R, Bocciolini M, Boezio M, *et al.* [CAPRICE Collab.]. 1996. *Astron. & Astrophys.* 309:L15

Barwick S W, Beatty J J, Bower C R, Chaput C, Coutu S, *et al.* [HEAT Collab.]. 1995. *Phys. Rev. Lett.* 75:390

Barwick S W, Beatty J J, Bhattacharyya A, Bower C R, Chaput C J, *et al.* [HEAT Collab.]. 1997. *Ap. J. Lett.* 482:191

Barwick S W, Beatty J J, Bower C R, Chaput C J, Coutu S, *et al.* [HEAT Collab.]. 1998. *Ap. J.* 498:779

Beach A S, Beatty J J, Bhattacharyya A, Bower C, Coutu S, *et al.* [HEAT Collab.]. 2001. *Phys. Rev. Lett.* 87:271101

Beatty J J, Bhattacharyya A, Bower C, Coutu S, Duvernois M A, *et al.* [HEAT Collab.]. 2004. *Phys. Rev. Lett.* 93:241102

Beischer B, von Doetinchem P, Gast H, Kirn T, and Schael S. 2009. *New J. Phys.* 11:105021

Bergström L. 2000. *Rep. Prog. Phys.* 63:793

Bergström L, Edsjö J, Gustafsson M, and Salati P. 2006. *J. Cosmol. Astropart. Phys.* 0605:6

Berkey G B and Shen C S. 1969. *Phys. Rev.* 188:1994

Bertone G, Hooper D, and Silk J. 2005. *Phys. Rep.* 405:279

Bertone G, Zentner A R, and Silk J. 2008. *Phys. Rev. D* 72:103517

Bindi V. 2010. *Nucl. Instrum. Methods Phys. Res. A* 617:462

Bionta R M, Blewitt G, Bratton C B, Casper D, and Ciocio A. 1987. *Phys. Rev. Lett.* 58:1494

Blasi P. 2009. *Phys. Rev. Lett.* 103:051104

Bloom E. 2010. "The Search for Dark Matter with Fermi: a Progress Report," *contribution to the Ninth UCLA Symposium on Sources and Detection of Dark Matter and Dark Energy in the Universe (Marina del Rey, CA)*

Blumenthal G R, Faber S M, Primack J R, and Rees M J. 1984. *Nature* 311:517

Boezio M, Carlson P, Francke T, Weber N, Suffert M, *et al.* [CAPRICE Collab.]. 1997. *Ap. J.* 487:415

Boezio M, Carlson P, Francke T, Weber N, Suffert M, *et al.* [CAPRICE Collab.]. 2000. *Ap. J.* 532:653

Boezio M, Bonvicini V, Schiavon P, Vacchi A, Zampa N, *et al.* [CAPRICE Collab.]. 2001. *Ap. J.* 561:787

Bogomolov E A, Lubyanaya N D, Romanov V A, Stepanov S V, and Shulakova M S. 1979. *Proc. of the 16th ICRC (Tokyo, Japan)* 1:330

Bottino M, Banday A J, and Maino D. 2008. *MNRAS* 389:1190

Bottino M, Banday A J, and Maino D. 2010. *MNRAS* 402:207

Bouquet A, Salati P, and Silk J. 1989. *Phys. Rev. D* 40:3168

Boylan-Kolchin M, Springel V, White S D M, Jenkins A, and Lemson G. 2009. *MNRAS* 398:1150

Buffington A, Schindler S M, and Pennypacker C R. 1981. *Ap. J.* 248:1179

Bullock J, Kaplinghat M, and Strigari L. 2010. In *Particle Dark Matter: Observations, Models, and Searches*, ed. G Bertone, pp. 38-56. Cambridge, UK: Cambridge Univ. Press

Buote D A, Gastaldello F, Humphrey P J, Zappacosta L, Bullock J S, *et al.* 2007. *Ap. J.* 664:123

Carosi G. 2004. *contribution to the XXIV Physics in Collisions Conference (PIC04) (Boston, USA)* (arXiv:physics/0409043)

Case G L and Bhattacharya D. 1998. *Ap. J.* 504:761

Cawley M F, Fegan D J, Harris K, Kwok P W, Hillas A M, *et al.* 1990. *Exp. Astron.* 1:173

Chang J, Adams J H, Ahn H S, Bashindzhagyan G L, Batkov K E, *et al.* [ATIC Collab.]. 2008a. *Adv. Sp. Res.* 42:431

Chang J, Adams J H, Ahn H S, Bashindzhagyan G L, Christl M, *et al.* [ATIC Collab.]. 2008b. *Nature* 456:362

Chi X, Cheng K S, and Young E C M. 1996. *Ap. J. Lett.* 459:83

Combes F. 1991. *Annu. Rev. Astron. Astrophys.* 29:195

Cole S, Lacey C G, Baugh C M, and Frenk C S. 2000. *MNRAS* 319:168

Couto S, Barwick S W, Beatty J J, Bhattacharya A, Bower C R, *et al.* [HEAT Collab.]. 1999. *Astropart. Phys.* 11:429

Cowsik R and Lee M A. 1979 *Ap. J.* 228:297

de Boer W, Sander C, Zhukov V, Gladyshev A V, and Kazakov D I. 2005. *Astron. & Astrophys.* 444:51

de Boer W, Sander C, Zhukov V, Gladyshev A V, and Kazakov D I. 2005. *Phys. Rev. Lett.* 95:209001

Delahaye T, Lineros R, Donato F, Fornengo N, Lavalle J, *et al.* 2009. *Astron. & Astrophys.* 501:821

Dermer C D. 2007 *AIP Conf. Proc.* 921:122

Desai S, Ashie Y, Fukuda S, Fukuda Y, Ishihara K, *et al.* [Super-Kamiokande Collab.]. 2004. *Phys. Rev. D* 70:083523. Erratum. 2004. *Phys. Rev. D* 70:109901

De Shong J A, Hildebrand R H, and Meyer P. 1964. *Phys. Rev. Lett.* 12:3

Dickey J M and Lockman F J. 1990. *Annu. Rev. Astron. Astrophys.* 28:215

Diemand J, Kuhlen M, and Madau P. 2007. *Ap. J.* 667:859

Diemand J, Kuhlen M, Madau P, Zemp M, Moore B, *et al.* 2008. *Nature* 454:735

Dimopoulos S and Georgi H. 1981. *Nucl. Phys. B.* 193:150

Dobler G and Finkbeiner D P. 2008. *Ap. J.* 680:1222

Dobler G, Finkbeiner D P, Cholis I, Slatyer T, and Weiner N. 2010. *Ap. J.* 717:825

Donato F, Fornengo N, and Salati P. 2000. *Phys. Rev. D* 62:043003

Donato F, Maurin D, Brun P, Delahaye T, and Salati P. 2009. *Phys. Rev. Lett.* 102:071301

DuVernois M A, Barwick S W, Beatty J J, Bhattacharyya A, Bower C R, *et al.* [HEAT Collab.]. 2001. *Ap. J.* 559:296

Esposito J A, Bertsch D L, Chen A W, Dingus B L, Fichtel C E, *et al.* 1999. *Ap. J. Supp.* 123:203

Essig R, Sehgal N, Strigari L E, Geha M, and Simon J D. 2010. *Phys. Rev. D* 82:123503

Fairbairn M and Zupan J. 2009. *J. Cosmol. Astropart. Phys.* 0907:001

Feng J L. 2010. *Annu. Rev. Astron. Astrophys.* 48:495

Ferenc D. [MAGIC Collab.]. 2005. *Nucl. Instrum. Methods Phys. Res. A* 553:274

Fichtel C E, Hartman R C, Kniffen D A, Thompson D J, Ogelman H, *et al.* 1975. *Ap. J.* 198:163

Finkbeiner D P. 2004. *Ap. J.* 614:186

Finkbeiner D P and Weiner N. 2007. *Phys. Rev. D* 76:083519

Gaisser T K and Levy E H. 1974. *Phys. Rev. D* 10:1731

Galli S, Iocco F, Bertone G, and Melchiorri A. 2009. *Phys. Rev. D* 80:023505

Gilmore R C, Madau P, Primack J R, Somerville R S, and Haardt F. 2009. *MNRAS* 399:1694

Gleeson L J and Axford W I. 1968. *Ap. J.* 154:1011

Glicenstein J F. 2010. “Indirect Dark Matter Searches with HESS,” *contribution to the International Conference on High Energy Physics (Paris, France)*

Gold B, Odegard N, Weiland J L, Hill R S, Kogut A, *et al.* 2010. *Ap. J. Supp.* *in press* (arXiv:1001.4555)

Golden R L, Horan S, Mauger B G, Badhwar G D, Lacy J L, *et al.* 1979. *Phys. Rev. Lett.* 43:1196

Goodman J, Ibe M, Rajaraman A, Shepherd W, Tait T, *et al.* 2011. *Nucl. Phys. B* 844:55

Grenier I A, Casandjian J-M, and Terrier R. 2005. *Science* 307:1292

Griest K and Kamionkowski M. 1990. *Phys. Rev. Lett.* 64:615

Guzik T G, Adams J H, Ahn H S, Bashindzhagyan G, Chang J, *et al.* [ATIC Collab.]. 2004. *Adv. Sp. Res.* 33:1763

Halzen F and Klein S R. 2010. *Rev. Sci. Instr. in press* (arXiv:1007.1247)

Haslam C G T, Salter C J, Stoffel H, and Wilson W E. 1982. *A&AS* 47:1

Hillas A M. 2005. *J. Phys. G* 31:95

Hinton J A. 2004. *New. Astron. Rev.* 48:331

Hinton J A and Hoffman W. 2009. *Annu. Rev. Astron. Astrophys.* 47:523

Hirata K, Kajita T, Koshiba M, Nakahata M, and Oyama Y. 1987. *Phys. Rev. Lett.* 58:1490

Hooper D, Finkbeiner D P, and Dobler G. 2007. *Phys. Rev. D* 76:083012

Hooper D and Baltz E A. 2008. *Annu. Rev. Nucl. Part. Sci.* 58:293

Hooper D and Zurek K M. 2008. *Phys. Rev. D* 77:083202

Hooper D, Spolyar D, Vallinotto A, and Gnedin N Y. 2010. *Phys. Rev. D* 81:103531

Hunter S D, Bertsch D L, Catelli J R, Dame T M, Digel S W, *et al.* 1997. *Ap. J.* 481:852

Jeltema T E, Kehayias J, and Profumo S. 2009. *Phys. Rev. D* 80:023005

Jungman G and Kamionkowski M. 1994. *Phys. Rev. D* 49:2316

Jungman G, Kamionkowski M, and Griest K. 1996. *Phys. Rep.* 267:195

Kabuki S, Uchida T, Kurosaka R, Okumura K, Enomoto R, *et al.* [CANGAROO Collab.]. 2003. *Proc. of the 28th ICRC (Tsukuba, Japan)* 5:2859

Kalashev O E, Semikoz D V, and Sigl G. 2009. *Phys. Rev. D* 79:063005

Kalberla M W and Kerp J. 2009. *Annu. Rev. Astron. Astrophys.* 47:27

Kamionkowski M and Turner M S. 1991. *Phys. Rev. D* 43:1774

Keshet U, Waxman E, and Loeb A. 2004. *J. Cosmol. Astropart. Phys.* 0404:6

Kiuchi R, Mori M, Bicknell G V, Clay R W, Edwards P G, *et al.* [CANGAROO Collab.]. 2009. *Ap. J.* 704:240

Klypin A A, Kravtsov A V, Valenzuela O, and Prada F. 1999. *Ap. J.* 522:82

Kobayashi T, Komori Y, Yoshida K, and Nishimura J. 2004. *Ap. J.* 601:340

Komatsu E, Smith K M, Dunkley J, Bennett C L, Gold B, *et al.* 2010. *Ap. J. Supp. in press* (arXiv:1001.4538)

Lagage P O and Cesarsky C J. 1983. *Astron. & Astrophys.* 118:L223

Lagage P O and Cesarsky C J. 1985. *Astron. & Astrophys.* 147:L127

Lin T, Finkbeiner D P, and Dobler G. 2010. *Phys. Rev. D* 82:023518

Linden T and Profumo S. 2010. *Ap. J. Lett.* 714:228

Lombardi S, Aleksic J, Barrio J A, Biland A, Doro M, *et al.* 2009. *Proc. of the 31st ICRC (Łódź, Poland)* (arXiv:0907.0738)

Lorimer D R, Faulkner A J, Lyne A G, Manchester R N, Kramer M, *et al.* 2006. *MNRAS* 372:777

Maeno T, Orito S, Matsunaga H, Abe K, Anraku K, *et al.* 2001. *Astropart. Phys.* 16:121

McCullough M and Fairbairn M. 2010. *Phys. Rev. D* 81:083520

Meng S, Slatyer T, and Finkbeiner D P. 2010. *Ap. J.* 724:1044

Mertsch P and Sarkar S. 2010. *J. Cosmol. Astropart. Phys.* 10:019

Mitchell J W, Barbier L M, Christian E R, Krizmanic J F, Krombel K, *et al.* 1996. *Phys. Rev. Lett.* 76:3057

Moiseev A, Yoshimura K, Ueda I, Anraku K, Golden R, *et al.* 1997. *Ap. J.* 474:479. Erratum. 1997. *Ap. J.* 482:1087

Moiseev A A, Deering P L, Hartman R C, Johnson T E, Nebel T R, *et al.* 2007. *Nucl. Instrum. Methods Phys. Res. A* 583:372

Moskalenko I V and Strong A W. 1998. *Ap. J.* 493:694

Moskalenko I V, Strong A W, Ormes J F, and Potgieter M S. 2002. *Ap. J.* 565:280

Moskalenko I V, Strong A W, and Reimer O. 2004. In *Cosmic Gamma-Ray Sources*, ed. K S Cheng & G E Romero, 304:279. *Astrophys. and Space Sci. Libr.* Dordrecht: Kluwer Acad.

Moskalenko I V, Porter T A, and Strong A W. 2006. *Ap. J. Lett.* 640:155

Moskalenko I V and Wai L L. 2007. *Ap. J. Lett.* 659:29

Müller D and Tang K K. 1990. *Proc. of the 21st ICRC (Adelaide, Australia)* 3:249

Navarro J F, Frenk C S, and White S D M. 1997. *Ap. J.* 490:493

Nelson A E and Spitzer C. 2010. *J. High Energy Phys.* 10:1

Niederste-Ostholt M, Belokurov V, Evans N W, Gilmore G, Wyse R F G, and Norris J E. 2009. *MNRAS* 398:1771

Ormes J F and Moiseev A. 2007. *AIP Conf. Proc.* 921:494

Peccei R D and Quinn H R. 1977. *Phys. Rev. Lett.* 38:1440

Perkins J S [VERITAS Collab.]. 2009. *AIP Conf. Proc.* 1085:569

Picozza P, Galper A M, Castellini G, Adriani O, Altamura F, *et al.* [PAMELA Collab.]. 2007. *Astropart. Phys.* 27:296

Porter T A and Protheroe R J. 1997. *J. Phys. G* 23:1765

Porter T A and Strong A W. 2005. *Proc. of the 29th ICRC (Pune, India)* 4:77

Porter T A, Moskalenko I V, Strong A W, Orlando E, and Bouchet L. 2008. *Ap. J.* 682:400

Prantzos N, Boehm C, Bykov A M, Diehl R, Ferriere K, *et al.* 2011. *Rev. Mod. Phys. in press* (arXiv:1009.4620)

Protheroe R J. 1982. *Ap. J.* 254:391

Ptuskin V S, Moskalenko I V, Jones F C, Strong A W, and Zirakashvili. 2006. *Ap. J.* 642:902

Pullen A R, Chary R R, and Kamionkowski M. 2007. *Phys. Rev. D* 76:063006

Punch M, Akerlof C W, Cawley M F, Chantell M, Fegan D J, *et al.* 1992. *Nature* 358:477

Read J I, Wilkinson M I, Evans N W, Gilmore G, and Kleyna J T. 2006. *MNRAS* 366:429

Reich P and Reich W. 1988. *A&AS* 74:7

Reiprich T H and Boehringer H. 2002. *Ap. J.* 567:716

Rudaz S and Stecker F W. 1988. *Ap. J.* 325:16

Salamon M H, McKee S, Musser J A, Tarle G, Tomasch A, *et al.* 1990. *Ap. J.* 349:78

Sánchez-Conde M A, Prada F, Lokas E L, Gómez M E, Wojtak R, and Moles M. 2007. *Phys. Rev. D* 76:123509

Sandick P, Spolyar D, Buckley M R, Freese K, and Hooper D. 2010. *Phys. Rev. D* 81:083506

Sandick P, Diemand J, Freese K, and Spolyar D. 2010. *J. Cosmol. Astropart. Phys. in press* (arXiv:1008.3552)

Schlegel D J, Bebek C, Heetderks H, Ho S, Lampton M, *et al.*. 2009. (arXiv:0904.0468)

Schubnell M. 2009. *Proc. 44th Rencontres de Moriond (Val d'Aosta, Italy)* (arXiv:0905.0444)

Scott P, Conrad J, Edsjö J, Bergström L, Farnier C, and Akrami Y. 2010. *J. Cosmol. Astropart. Phys.* 1001:031

Shen C S and Berkey G B. 1968. *Phys. Rev.* 5:171

Shen C S. 1970 *Ap. J. Lett.* 162:181

Shikaze Y, Haino S, Abe K, Fuke H, Hams T, *et al.* 2007. *Astropart. Phys.* 28:154

Silk J and Srednicki M. 1984. *Phys. Rev. Lett.* 53:624

Silk J, Olive K A, and Srednicki M. 1985. *Phys. Rev. Lett.* 55:257

Simon J D and Geha M. 2007. *Ap. J.* 670:313

Simon J D, Geha M, Minor Q E, Martinz G D, Kirby E N, *et al.*. 2010. *Ap. J. in press* (arXiv:1007.4198)

Simon M, Molnar A, and Roesler S. 1998. *Ap. J.* 499:250

Somerville R S. 2002. *Ap. J. Lett.* 572:23

Springel V, Wang J, Vogelsberger M, Ludlow A, Jenkins A, *et al.* 2008. *MNRAS* 391:1685

Sreekumar P, Bertsch D L, Dingus B L, Esposito J A, Fichtel C E, *et al.* 1998. *Ap. J.* 494:523

Stawarz L, Petrosian V, and Blandford R D. 2010. *Ap. J.* 710:236

Stecker F W, Rudaz S, and Walsh T F. 1985. *Phys. Rev. Lett.* 55:2622

Stecker F W, Malkan M A, and Scully S T. 2006. *Ap. J.* 648:774

Stecker F W, Hunter S D, and Kniffen D A. 2008. *Astropart. Phys.* 29:25

Stone E C, Frandsen A M, Mewaldt R A, Christian E R, Margolies D, *et al.* 1998. *Sp. Sci. Rev.* 86:1

Strigari L E, Bullock J S, Kaplinghat M, Simon J D, Geha M, *et al.*. 2008. *Nature* 454:1096

Strong A W and Moskalenko I V. 1998. *Ap. J.* 509:212

Strong A W, Moskalenko I V, and Reimer O. 2000. *Ap. J.* 537:763. Erratum. 2000. *Ap. J.* 541:1109

Strong A W, Moskalenko I V, and Reimer O. 2004. *Ap. J.* 613:956

Strong A W, Moskalenko I V, and Reimer O. 2004. *Ap. J.* 613:962

Strong A W. 2007. *Astrophys. Sp. Sci.* 309:35

Strong A W, Moskalenko I V, and Ptuskin V S. 2007. *Annu. Rev. Nucl. Part. Sci.* 57:285

Tarlé G and Schubnell M. 2001. *Sp. Sci. Rev.* 99:95

Tauber J A, Mandolesi N, Puget J-L, Banos T, Bersanelli M, *et al.* 2010. *Astron. & Astrophys.* 520:1

Tavani M, Barbiellini G, Argan A, Bulgarelli A, Caraveo P, *et al.* [AGILE Collab.]. 2008. *Nucl. Instrum. Methods Phys. Res. A* 588:52

Teegarden B J, Watanabe K, Jean P, Knöldlseder J, Lonjou V, Roques J P, *et al.* 2005. *Ap. J.* 621:296

Thompson D J, Bertsch D L, Fichtel C E, Hartman R C, Hofstadter R, *et al.* 1993. *Ap. J. Supp.* 86:629

Tollerud E J, Bullock J S, Strigari L E, and Willman B. 2008. *Ap. J.* 688:277

Trotta R, Jóhannesson G, Moskalenko I V, Porter T A, Ruiz de Austri R, and Strong A W. 2011. *Ap. J. in press* (arXiv:1011.0037)

Turner M S. 1986. *Phys. Rev. D* 34:1921

Vikhlinin A, Kravtsov A, Forman W, Jones C, Markevitch M, *et al.* 2006. *Ap. J.* 640:691

Vitale V and Morselli A. 2009. *Proc. Second Fermi Symp. eConf Proc. C0911022 (Washington DC, USA)* (arXiv:0912.3838)

Wang P. 2009. “The Search for Dark Matter Galactic Satellites with *Fermi*-LAT,” *contribution to the April Meeting of the American Physical Society, (Denver, CO)*

Waxman E and Loeb A. 2000. *Nature* 405:L156

Weekes T C, Badran H, Biller S D, Bond I, Bradbury S, *et al.* [VERITAS Collab.]. 2002. *Astropart. Phys.* 17:221

Weinberg S. 1978. *Phys. Rev. Lett.* 40:223

Wilczek F. 1978. *Phys. Rev. Lett.* 40:279

York D G, Adelman J, Anderson J E Jr, Anderson S F, Annis J, *et al.* [SDSS Collab.]. 2000. *Astron. J.* 120:1579

Zavala J, Springel V, and Boylan-Kolchin M. 2010. *MNRAS* 405:593

Zemp M. 2009. *Mod. Phys. Lett. A* 24:2291